Gondwana Research 129 (2024) 36–52

Contents lists available at ScienceDirect

Gondwana Research

journal homepage: www.elsevier.com/locate/gr

The influence of lithospheric inheritance and Cenozoic magmatism on Phanerozoic rock cooling in the São Francisco Craton and adjacent orogens

Edgar do Amaral Santos [a,*], Andréa Ritter Jelinek [b], Frederico Antônio Genezine [c], Daniel Stockli [d]

[a] Programa de Pós-Graduação em Geociências, Universidade Federal do Rio Grande do Sul, Brazil
[b] Instituto de Geociências, Universidade Federal do Rio Grande do Sul, Brazil
[c] Instituto de Pesquisas Energéticas e Nucleares, Centro do Reator de Pesquisas, Brazil
[d] University of Texas at Austin, United States

ARTICLE INFO

Article history:
Received 8 July 2023
Revised 13 November 2023
Accepted 9 December 2023
Available online 14 December 2023
Handling Editor: A. Festa

ABSTRACT

The South American Platform encompasses the São Francisco Craton (SFC) and the Araçuaí-Ribeira orogenic system (AROS) located in the eastern Brazil. These geologic domains hold records of differential exhumation, sedimentation, volcanic activity, and post-rift reactivation of faults and shear zones. Therefore, these terranes provide outstanding opportunities for studying the dynamics of lithospheric processes, particularly in their interaction zones, characterized by the transition from cratonic to orogenic lithosphere. To investigate the processes involved in the contrasting behavior of the upper crust, we provide 23 new apatite fission track (AFT) ages and thermal histories from the northern segment of the AROS and from the eastern area of the SFC. The AFT ages range from 154.4 ± 20.1 and 37.1 ± 3.0 Ma and the mean track lengths range from 10.9 and 13.2 μm. We compiled thermal information from previous thermochronological analysis from 357 sites and constructed inverse distance weighted maps that depict the spatial distribution of AFT ages and the temperature evolution from 360 to 30 Ma. The results indicate that the SFC experienced its final exhumation within the apatite partial annealing zone (APAZ) at temperatures ranging from 110 °C to 60 °C during the late Paleozoic. In contrast, the AROS went through its last cooling within the APAZ during the Mesozoic or even in the Cenozoic. This suggests that reactivation and reheating, possibly associated with the South Atlantic rift, influenced the orogenic basement of the passive margin. We highlight that the reheating associated to the Abrolhos magmatic province in the northern segment of the AROS caused the youngest AFT ages of the study area. Our work demonstrates the importance of considering contrasting rheology when analyzing regional exhumation patterns, the structural fabric of orogens through reactivation of crustal discontinuities generating heating and exhumation, and how volcanism can disrupt the thermal record, inducing crustal reheating.

1. Introduction

A range of mechanisms, spanning from deep within the Earth, such as mantle dynamics (Dávila et al., 2023) and tectonics (Val et al., 2018), to surface climate conditions (Jepson et al., 2021) govern lithospheric processes. These mechanisms are further influenced by factors like rheology (Fonseca et al., 2021), the presence of crustal discontinuities (do Amaral Santos et al., 2022), and volcanism (Hueck et al., 2018; do Amaral Santos et al., 2023).

A significant lithospheric discontinuity results from the collision of various terranes during continental amalgamation. Eastern Brazil offers an ideal case study for investigating lithospheric dynamics due to its composition, featuring the São Francisco Craton (SFC) and Neoproterozoic-Cambrian orogenic areas. The SFC is one of the five old and differentiated components of the South American lithosphere, characterized by a shape resembling a horse's head (Fig. 1). It extends deep into the interior of eastern Brazil and forms the basement of the South Atlantic coast. Along the southeastern border of the SFC lies the Araçuaí and the Ribeira orogens, together forming the intricate Neoproterozoic-Cambrian orogenic system known as the Araçuaí-Ribeira orogenic system (AROS; Alkmim et al., 2017; Heilbron et al., 2017b), which was consolidated during the amalgamation of West Gondwana (Degler et al., 2017). Subsequently, during the Cretaceous, the AROS underwent rifting, and its rocks became integral to the basement of the continental margin established with the opening of the South

* Corresponding author.
E-mail addresses: edgar.amaral@ufrgs.br, santos.eas@gmail.com (E. do Amaral Santos).

https://doi.org/10.1016/j.gr.2023.12.003
1342-937X/

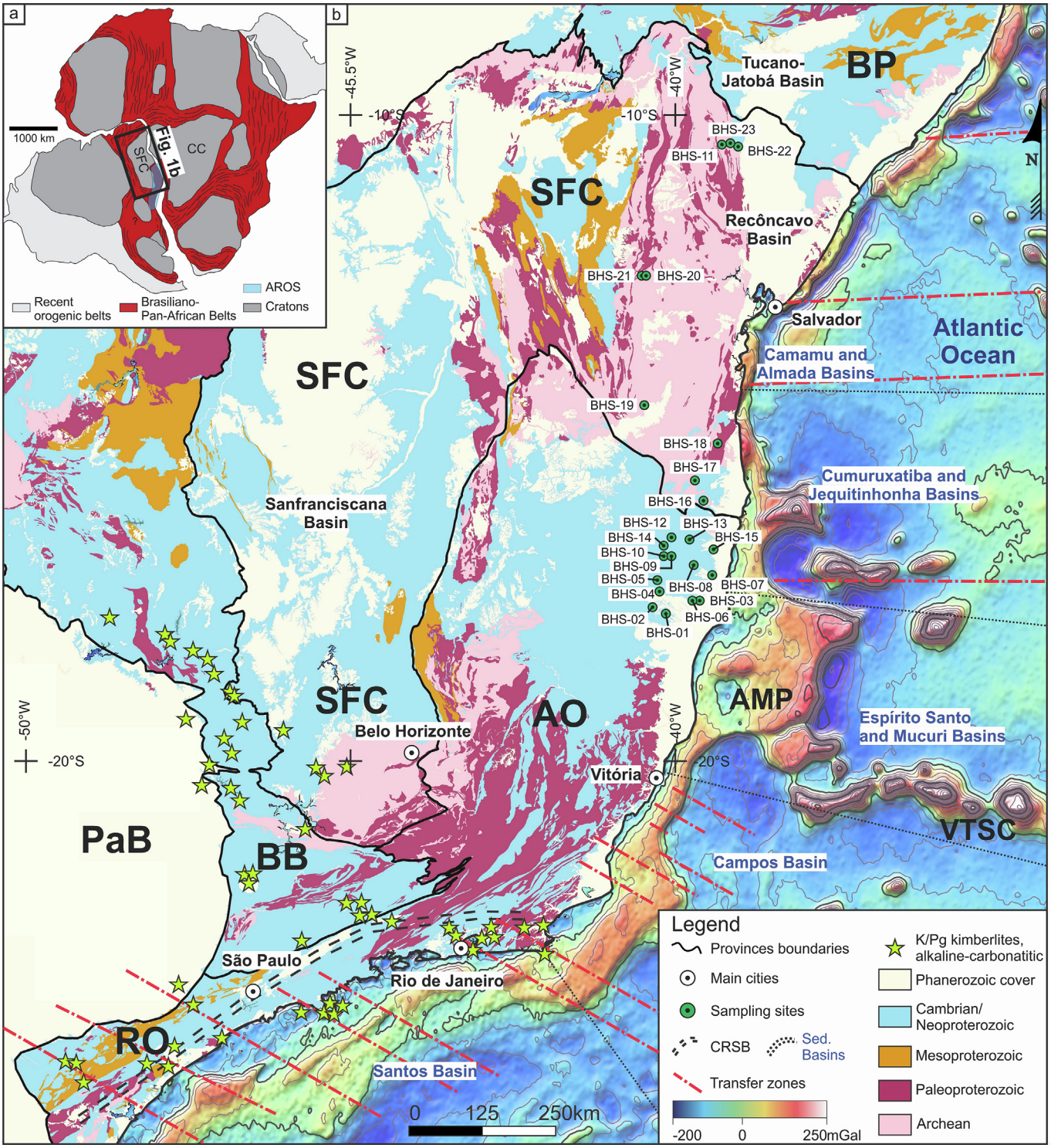

Fig. 1. a) West gondwana map depicting the cratons, some orogenic systems formed during the west gondwana amalgamation, and the recent orogens (after Oriolo et al., 2017). SFC: São Francisco Craton; CC: Congo Craton; AROS: Araçuaí-Ribeira orogenic system. b) Geologic map of the study area in eastern Brazil (after Dalton de Souza et al., 2003; Perrota et al., 2005; Heilbron et al., 2016; Silva et al., 2020), evidencing the limits of the São Francisco Craton and the adjacent Araçuaí Orogen (AO), Ribeira Orogen (RO), Brasília Orogen (BB), the Borborema Province (BP), and the intracratonic Paraná (PaB), Sanfranciscana, Recôncavo-Tucano-Jatobá Basins, as well as the Continental Rift of Southeastern Brazil (CRSB) (Riccomini et al., 2004) and the Cretaceous/Paleogene kimberlites and alkaline-carbonatitic rocks. The offshore region displays the gravity anomaly map of the South Atlantic Ocean seafloor (Sandwell et al., 2014) eastward of the study area, evidencing the Abrolhos Magmatic Province (AMP), the Vitória-Trindade seamount chain (VTSC), and the Cretaceous/Cenozoic marginal basins (Mohriak and Fainstein, 2012).

Atlantic Ocean (Nürnberg and Müller, 1991; Chang et al., 1992; Torsvik et al., 2009).

To understand the evolution of these distinct pieces of lithospheres, especially after its consolidation, we have selected the apatite fission track method (AFT; Price and Walker, 1963; Donelick et al., 2005) as our investigative tool. This method effectively constrains thermal information within a temperature range of approximately 120 to 60 °C, corresponding to the upper few

kilometers of the crust at depths ranging from 5 to 2 km (Gleadow and Duddy, 1981; Gleadow et al., 1986; Green et al., 1986). While the eastern Brazilian margin has a substantial number of previously analyzed samples, there still exist data gaps that require attention. We collected an additional 23 crucial basement samples in the underinvestigated northern region of the AROS and in the eastern SFC for subsequent AFT analyses, some of which have been previously analyzed for apatite and zircon (U-Th)/He thermochronology (do Amaral Santos et al., 2022). The AFT ages available in the literature and thermal information from 357 samples were put together with the new data to create inverse distance-weighted (IDW) maps. One of these maps depicts the spatial distribution of AFT ages, while 12 maps illustrate the temperature evolution from 360 to 30 Ma throughout the region. These maps were further analyzed and discussed along with geological data available in the literature, focusing on local and regional lithospheric processes. Our study aims to understand how the spatial distribution of AFT ages behaves in this transitional zone, how the thermal history recorded evolved through time and temperature, and which cooling and reheating events the area recorded. Then, we looked for evidence for the control of rheology, reactivation of crustal discontinuities, and volcanism on crustal exhumation, considering a regional geodynamic perspective.

2. Geologic framework

The study area extends from southeastern to northeastern Brazil, encompassing cratonic and orogenic terranes known as São Francisco Craton and the Araçuaí-Ribeira orogenic system, along with the eastern continental margin of the South America (Fig. 1).

The SFC was formerly a component of a larger cratonic lithosphere, alongside the Congo Craton, now situated in the African continent. These cratons remained connected until their separation during the opening of the South Atlantic Ocean in the Lower Cretaceous (Alkmim and Martins-Neto, 2012; Heilbron et al., 2017a). The exposed basement units of the SFC are older than 1.8 Ga, while the cratonic cover consists of sequences younger than 1.8 Ga (de Almeida, 1977). Archean TTG-gneisses, granitoids, greenstone belts, Paleoproterozoic plutons, and supracrustal successions characterize the basement units. The cratonic cover encompasses Proterozoic and Phanerozoic sedimentary sequences (Alkmim and Marshak, 1998; Alkmim and Martins-Neto, 2012). Surrounding this craton are the Brasiliano orogens, a series of orogenic systems formed during the amalgamation of the West Gondwana continent. This work analyzed the AROS, which is located southeast and south of the craton, composed by the Araçuaí and Ribeira orogens (Fig. 1; de Almeida, 1977).

The Araçuaí Orogen was formed during the Neoproterozoic to the Cambrian through the interaction of the SFC and the Congo Craton in a confined setting, where these cratons formed an embayment (Alkmim et al., 2006; Heilbron et al., 2017a; Pedrosa-Soares et al., 2011, 2008). The Araçuaí Orogen represents the Brazilian portion of the larger Araçuaí-West Congo Orogen (Alkmim et al., 2017). During the orogeny, parts of the previous cratonic basement units, such as crystalline rocks older than 1.8 Ga and the Paleo to Mesoproterozoic rift to rift-sag successions of the Espinhaço Supergroup, were deformed by the collisional event. The orogen is also composed by Neoproterozoic to Cambrian passive margin units (Macaúbas Group; e.g. Souza et al., 2019), *syn*-orogenic sequences, and crustal-derived granitic intrusions. The *syn*-metamorphic climax of the granitic plutons dates to ca. 590 to 530 Ma (Pedrosa-Soares and Wiedemann-Leonardos, 2000; Pedrosa-Soares et al., 2001; Alkmim et al., 2017).

Located southward of the SFC, the Ribeira Orogen resulted from multiple collisional episodes during the Neoproterozoic to Cambrian (Heilbron and Machado, 2003). This orogen consists of four tectono-stratigraphic terranes, including a reworked cratonic basement of the external sector along with intra-cratonic basins and a passive margin unit, active margin sequences, continental magmatic arcs, and a series of granites that intruded the basement, and supracrustal units (Heilbron et al., 2020). Terrane docking and reworking have played a significant role in this orogen. At the same time, the structural fabric of this orogen is characterized by shear zones and large-scale folds, with metamorphic imprints ranging from 630 to 510 Ma (Heilbron et al., 2017b).

Several basin depocenters developed within the Gondwana continent from the Ordovician onwards, such as the Paraná and Sanfranciscana basins (Linol et al., 2015). The Paraná Basin, located southwest of the study area, consists of six supersequences separated by regional unconformities. Transgressive-regressive cycles characterize the first three sequences of Ordovician to Permian/Triassic ages, and the last three sequences comprise continental volcano-sedimentary units of Triassic to Cretaceous ages (Milani et al., 1998, 2007a; Scherer et al., 2023). The Sanfranciscana basin, located within the SFC, developed from the Carboniferous/Permian to the Cretaceous, comprising glacial-marine and continental desertic environments associated with volcanic extrusions (Campos and Dardenne, 1997; Sgarbi and de Sgarbi, 2001; Zalán and Silva, 2007).

The rifting of the West Gondwana and the subsequent formation of the continental margin to the east of the SFC and AROS was followed by the opening of the South Atlantic Ocean during the Lower Cretaceous (Mohriak et al., 2008). On both segments, cratonic or non-cratonic basements, lie Cretaceous to Cenozoic sedimentary deposits that are intruded by Paleocene to Eocene volcanic rocks (Mohriak and Fainstein, 2012). The volcanic record in the region is notable for the significant Abrolhos Magmatic Province (Stanton et al., 2021), as well as the Vitória-Trindade seamount chain. Additionally, a series of kimberlite and alkaline-carbonatitic plutons intruded both the margin and the interior of the continent in southeastern Brazil during the Cretaceous and Paleogene (Takenaka et al., 2023).

The Continental Rift of Southeastern Brazil (CRSB) developed during the Paleogene, forming an elongated narrow trough nearly 900 km long (Riccomini, 1990; Riccomini et al., 2004; Zalán and De Oliveira, 2005). This tectonic feature is mainly parallel to the present-day coastline and the Neoproterozoic shear zones of the Ribeira Orogen. These shear zones were reactivated as normal faults, generating sedimentary basins and as strike-slip afterward (Pinheiro and Cianfarra, 2021). As the rift developed, volcanic alkaline magmas erupted near the border of the rift (Riccomini et al., 2004, 2005).

3. Methods

3.1. Apatite fission track thermochronology

For the apatite fission track (AFT) thermochronology, this study collected 23 basement samples from the SFC and AROS regions. Our focus was on crystalline lithologies rich in apatite such as granites and gneisses. Some of these samples had previously undergone analysis for zircon and apatite (U-Th)/He thermochronology (do Amaral Santos et al., 2022), which this study integrated (Supplementary Data, Table S1 and S2). Table 1 contains information regarding the lithology, sample locations, altitudes, and the methods employed in each sample.

The AFT method relies on the accumulation of fission tracks resulting from the spontaneous fission of ^{238}U (Price and Walker, 1963; Fleischer and Price, 1964). By analyzing the areal density of tracks in apatite and in an external detector we can determine

Table 1
Details from samples analyzed in this study. Coordinates in decimal degree; AHe and ZHe data published in do Amaral Santos et al. (2022) and available in Supplementary Data, Table S1 and S2. AFT: Apatite Fission Track; AHe: Apatite (U-Th)-He dating; ZHe: Zircon (U-Th)/He dating.

Sample	Lithology	Latitude (° S)	Longitude (° W)	Elevation (m)	Method
BHS-01	Granitoid	17.717500	40.141111	169	AFT
BHS-02	Granitoid	17.615278	40.346667	252	AFT, ZHe, AHe
BHS-03	Granitoid	17.515278	39.650556	24	AFT
BHS-04	Granitoid	17.371667	40.231667	149	AFT
BHS-05	Granitoid	17.188889	40.280556	227	AFT
BHS-06	Granitoid	17.512222	39.705000	86	AFT, ZHe, AHe
BHS-07	Granitoid	17.131667	39.433333	36	AFT
BHS-08	Granitoid	16.957222	39.716111	82	AFT
BHS-09	Granitoid	16.827500	40.056667	197	AFT
BHS-10	Granitoid	16.837222	40.141667	207	AFT, Zhe
BHS-11	Granitoid	10.468889	39.268611	450	AFT
BHS-12	Granitoid	16.571111	40.089167	292	AFT, ZHe
BHS-13	Granitoid	16.575000	39.781667	187	AFT, ZHe, AHe
BHS-14	Granitoid	16.659167	40.175278	293	AFT
BHS-15	Granitoid	16.725278	39.410000	80	AFT, ZHe, AHe
BHS-16	Granitoid	15.968889	39.561944	82	AFT
BHS-17	Granitoid	15.668889	39.691111	119	AFT, ZHe, AHe
BHS-18	Granitoid	15.083333	39.340556	90	AFT
BHS-19	Granitoid	14.493333	40.467222	838	AFT
BHS-20	Granitoid	12.509167	40.449444	305	AFT
BHS-21	Granitoid	12.493333	40.506667	317	AFT
BHS-22	Granitoid	10.489444	39.067778	385	AFT
BHS-23	Granitoid	10.465000	39.146111	449	AFT

the AFT age and by analyzing the length of horizontal confined fission tracks we can reconstruct the thermal history experienced by each sample within the range of this thermochronometer (Reiners et al., 2017). The thermal models derive from AFT data after simulations of a mathematical model that represents time–temperature dependance of annealing (Gallagher, 2012). These data are composed, among other parameters, of a collection of measured horizontal confined fission tracks (MTL) that experienced a portion of the thermal history. For the AFT method, the fission tracks remain preserved below 120 °C over geological timescales, corresponding to upper crustal temperatures. However, at temperatures between 120 and 60 °C (Green et al., 1989), the tracks undergo shrinkage due to thermal annealing, with the temperature, chemical composition, and radiation damage acting as controlling factors (Donelick et al., 2005; Tagami and O'Sullivan, 2005), defining the Apatite Partial Annealing Zone (APAZ).

Standard crushing, sieving, and hand-picking techniques concentrated the apatite crystals (Kohn et al., 2019). This study utilized the external detector method (EDM; Hurford, 1990) and neutron irradiation in the CNEN-IPEN reactor in São Paulo, Brazil. The apatite crystals were embedded in epoxy resin, polished, and subjected to chemical etching with HNO_3 5.5 M at 21 °C for 20 s (Carlson et al., 1999; Donelick et al., 2005) to reveal spontaneous tracks. Low-U muscovite sheets were affixed to the apatite mounts, U-doped glass dosimeters (CN5), and Durango age standards. To expose induced tracks, 48 % HF at 20 ℃ for 18 min etched the mica sheets.

AFT dating and track length measurements were conducted at the Labmodel, a thermochronology facility at the Universidade Federal do Rio Grande do Sul, Brazil. The analysis was assisted using a Leica CTR 6000 microscope at a magnification of 1000x (dry). A minimum of 20 grains were used for AFT age calculation, with only one sample not meeting this criterion. The ς calibration method was employed to calibrate the AFT ages (Hurford and Green, 1983), and age homogeneity was evaluated using the chi-squared test (Galbraith, 1981) in RadialPlotter 9.4 (Vermeesch, 2009). A length-frequency histogram of AFT data (n > 50) was obtained for 19 representative samples, while less representative histograms (50 > n > 10) were obtained for three samples.

3.2. Inverse modeling

Inverse modeling was performed for 22 samples using the QTQt 5.8.0 software (Gallagher, 2012), with D_{par} and c-axis projection (Ketcham et al., 2007) employed as parameters to model AFT data (Ketcham et al., 2007). For inverse modeling, the radiation damage accumulation and annealing models for zircon (Guenthner et al., 2013) and apatite (Flowers et al., 2009) were utilized to model (U-Th)/He data of zircon and apatite, respectively.

The present-day surface temperature was constrained to 20 ± 10 °C. When considering only AFT data, the prior temperature was set at 70 ± 70 °C, whereas it was set at 100 ± 100 °C when including ZHe data. The oldest AFT or ZHe/AHe age of each sample was used as a prior for time with an uncertainty of $t_o \pm t_o$, and the maximum gradient (∂T/∂t) was set at 30 ℃/m.y. Initial runs of 30,000 iterations were used to define the values for the MCMC algorithm. Runs of at least 200,000 post-burn-in iterations were then defined with the appropriate values for inverse modeling. This work analyzed the expected model defined by curves that represent the 95% credible interval and the weighted mean path of each model.

3.3. Data kriging

To evaluate the AFT age of all available samples in the literature across SFC and AROS and to assess the evolution of basement temperature in this region, we employed inverse distance weighted (IDW) maps created using ArcGIS 10.3. The map illustrating the AFT ages was constructed based on the AFT central ages of 728 sites (Supplementary Data, Table S3). The IDW maps depicting the temperature evolution were generated using temperature data collected from the weighted mean path of each model at 12 specific time intervals (360 to 30 Ma) acquired from 357 sites, including thermal models created in this study and those available in the literature (Supplementary Data, Table S4). The analysis of thermal histories predominantly relied on AFT; however, some studies integrated this thermochronometer with other geochronometers and thermochronometers, such as (U-Th)/He in zircon and apatite and U-Pb in zircon (Franco et al., 2005; Hiruma et al., 2010; Cogné

et al., 2011, 2012; Doranti-Tiritan, 2013; Jelinek et al., 2014, 2020; Engelmann de Oliveira et al., 2016; Soares et al., 2016; Amaral-Santos et al., 2019; Krob et al., 2019; Van Ranst et al., 2020; Fonseca et al., 2021, 2022, 2023; Gezatt et al., 2021; Costa, 2022; do Amaral Santos et al., 2022). Notably, one study used constraints to replicate present-day temperature conditions for modeling in low-temperature environments, which may bias the models to force low-temperature paths (Krob et al., 2019).

4. Results

4.1. AFT ages and MTL

The new AFT data from 23 analyzed sites in the northern AROS and SFC are summarized in Table 2 and Fig. 2. The new AFT central ages vary from 154.4 ± 20.1 to 37.1 ± 3.0 Ma, between the Jurassic and the Eocene (Fig. 2). The AFT ages of samples collected in the orogenic domain vary from 125.6 to 37.1 Ma and are younger. In contrast, the cratonic area exhibits older ages, spanning from 154.4 to 103.8 Ma, except for two samples recording 77.0 and 77.2 Ma (Fig. 2). This data set displays a positive correlation between AFT ages and the distance to the coast as well as a positive correlation between AFT ages and D_{par} (Supplementary Data, Figs. S1 and S2). Additionally, the samples BHS-02 and BHS-13 display AFT ages younger than their AHe ones.

Track-length and c-axis angle data were acquired from 22 samples, while only one sample lacked this information (Table 2). Nineteen samples have more than 60 horizontal confined fission-track lengths measured, whereas three samples have yet to reach 40 tracks measured. The MTL falls within the short to intermediate range (10.9 to 13.2 μm), with most tracks measuring approximately 11 to 12 μm. This data set displays a negative correlation between AFT ages and MTL (Supplementary Data, Fig. S3). The MTL exhibits a unimodal distribution with narrow standard deviation and negative skewness (Supplementary Data, Fig. S4).

4.2. Thermal history patterns and temperature variations: Insights from thermal models and data kriging

Based on the new thermal models constructed from samples of this study, three distinct groups were identified (Fig. 3 and Supplementary Data, Fig. S5):

(i) Slow continuous cooling from the Paleozoic onwards until present (BHS-01, 09, 14, and 16) or samples recording only slow continuous cooling lacking thermal signals before 110 Ma (BHS-03, 05, 07, and 15).
(ii) The onset of slow cooling from the Paleozoic to the Upper Cretaceous within the APAZ, followed by a rapid cooling event starting in Paleogene-Neogene until present from the upper portion of the APAZ to surface conditions (BHS-04, 08, 11, and 19 to 23).
(iii) An initial fast cooling episode in the Cretaceous from temperatures higher than the APAZ succeeded by reheating 10 to 25 °C during the Paleogene and, subsequently, a final cooling to present-day surface conditions (BHS-02, 06, 10, 13, 17, and 18).

Considering the new and the compiled AFT data used for constructing the IDW map (Fig. 4), the AFT age spatial distribution depicted in this map reveals older AFT ages in both northern and southern segments of the SFC. The northern portion displays Permian to Triassic ages, while the southern region primarily encompasses ages within the Triassic to Jurassic. Jurassic to Lower Cretaceous ages characterize the transitional region from the craton to the adjacent orogens.

Table 2
New Apatite Fission Track data from the Araçuaí Orogen and the São Francisco Craton, in southeastern to northeastern Brazil.

Sample	N #	ρs (Ns) (×10^5)	ρi (Ni) (×10^5)	ρd (Nd) (×10^5)	P (χ2) (%)	U (μg/g)	Centr. Age ± 1σ (Ma)	n #	MTL (μm)	Std. Dev. (μm)	P.MTL (μm)	P.Std. Dev. (μm)	Dpar (μm)	Skewness #
BHS-01	25	10.68 (156)	13.01 (190)	21.30 (27164)	0.99	7.8	116.5 ± 14.0	100	12.1	1.71	13.5	1.34	1.51	−0.14
BHS-02	25	6.04 (330)	12.77 (697)	14.54 (18586)	0.97	11.1	46.1 ± 3.7	100	12.5	1.58	13.7	1.26	1.52	−0.13
BHS-03	25	12.65 (148)	27.52 (322)	21.30 (27164)	0.79	16.4	65.5 ± 7.2	11	12.7	1.92	13.6	1.87	1.46	−1.09
BHS-04	25	15.99 (331)	41.98 (869)	14.54 (18586)	1.00	36.7	37.1 ± 3.0	101	11.3	1.87	13.1	1.25	1.43	−0.19
BHS-05	25	5.53 (142)	10.82 (278)	14.54 (18586)	0.95	9.4	49.7 ± 5.5	77	12.7	1.61	14.0	1.14	1.48	−0.66
BHS-06	25	4.15 (164)	5.22 (206)	14.54 (18586)	0.99	4.6	77.3 ± 8.5	70	13.2	1.80	14.3	1.26	1.5	−0.61
BHS-07	25	7.09 (317)	15.28 (683)	14.54 (18586)	0.88	13.3	45.2 ± 3.6	100	12.8	1.59	13.9	1.10	1.45	−0.65
BHS-08	25	13.84 (256)	10.97 (203)	14.54 (18586)	0.5	9.6	122.1 ± 12.2	100	11.6	1.97	13.2	1.41	1.7	−0.12
BHS-09	25	10.68 (156)	13.01 (190)	21.30 (27164)	1.00	7.8	116.5 ± 14.0	70	12.3	1.93	13.5	1.65	1.61	−0.24
BHS-10	25	16.92 (330)	17.54 (342)	14.54 (18586)	0.89	15.3	93.6 ± 8.4	100	12.0	1.69	13.3	1.32	1.63	−0.03
BHS-11	25	13.29 (299)	15.73 (354)	21.30 (27164)	0.96	9.4	119.8 ± 10.8	100	10.9	1.68	12.6	1.33	1.59	0.03
BHS-12	14	8.38 (88)	8.38 (88)	14.54 (18586)	0.50	7.3	97.0 ± 15.5	*	*	*	*	*	*	*
BHS-13	25	7.40 (290)	9.21 (361)	14.54 (18586)	0.61	8.0	78.0 ± 7.0	100	12.4	1.59	13.7	1.10	1.65	−0.53
BHS-14	25	6.94 (460)	7.828 (519)	21.30 (27164)	0.28	4.7	125.6 ± 10.0	66	12.3	1.88	13.5	1.53	1.65	−0.84
BHS-15	25	14.73 (383)	36.31 (944)	21.30 (27164)	0.72	21.6	57.8 ± 4.6	100	12.6	1.61	13.9	1.13	1.61	−0.41
BHS-16	25	6.11 (113)	6.70 (124)	21.30 (27164)	1.00	4.0	129.2 ± 18.1	15	11.8	1.56	13.2	1.20	1.77	−0.1
BHS-17	25	7.81 (225)	7.36 (212)	21.30 (27164)	0.97	4.4	150.2 ± 16.5	101	11.9	1.75	13.3	1.33	1.58	−0.16
BHS-18	25	7.26 (283)	9.13 (356)	14.54 (18586)	0.944	8.0	77.2 ± 6.9	72	11.4	1.91	13.0	1.36	1.53	0.08
BHS-19	25	22.00 (220)	30.10 (301)	21.30 (27164)	0.95	17.9	103.8 ± 10.4	76	11.9	1.89	13.4	1.24	1.54	−0.37
BHS-20	25	22.90 (229)	42.30 (423)	21.30 (27164)	1.00	25.2	77.0 ± 6.9	100	11.5	1.67	12.9	1.54	1.46	−0.06
BHS-21	25	20.75 (220)	18.02 (191)	14.54 (18586)	1.00	15.7	111.6 ± 12.3	100	11.2	1.67	13.0	1.25	1.48	0.24
BHS-22	25	24.20 (242)	18.80 (188)	14.54 (18586)	1.00	16.4	124.6 ± 13.7	37	11.2	2.07	13.0	1.26	1.49	0.34
BHS-23	25	13.08 (187)	8.18 (117)	14.54 (18586)	1.00	7.1	154.4 ± 20.1	99	11.8	1.66	13.1	1.40	1.48	0.13

N: number of apatite crystals analyzed to determine track densities; ρs: measured spontaneous track density; Ns: number of spontaneous tracks counted; ρi: measured induced track density; Ni: number of induced tracks counted; ρd: track density measured in external detector adjacent to glass dosimeter during irradiation; Nd: number of tracks counted in determining ρd; P (χ2): chi-squared probability; n: number of confined track lengths measured; * no horizontal confined track length measured; Centr. Age: Central Age; Std. Dev.: Standard Deviation; P.MTL: Projected mean track length; P.Std. Dev.: Standard Deviation of Projected mean track length.
Apatite ages calculated using a zeta of 134.41 ± 6.19 for CN5 glass on Brazil reactor. Analyst: Edgar do Amaral Santos.

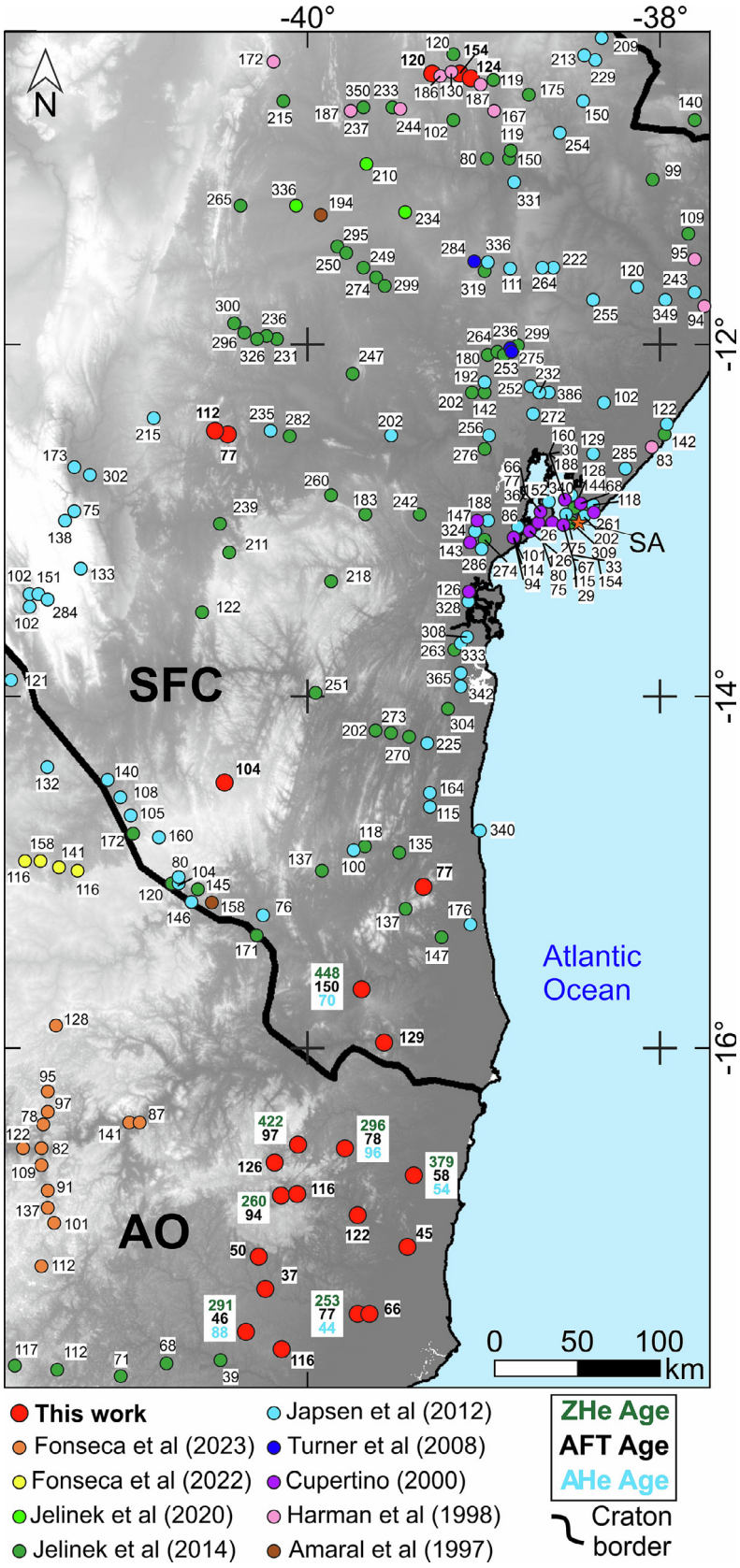

Fig. 2. Distribution of the new AFT ages of this data set along with AFT, AHe, and ZHe ages available in the literature from the northern Araçuaí Orogen (AO) and the São Francisco Craton (SFC) (Amaral et al., 1997; Harman et al., 1998; Cupertino, 2000; Turner et al., 2008; Japsen et al., 2012; Jelinek et al., 2014, 2020; do Amaral Santos et al., 2022; Fonseca et al., 2022, 2023). Results of this study are displayed in bold and is the only work to incorporate both ZHe and AHe data in the area.

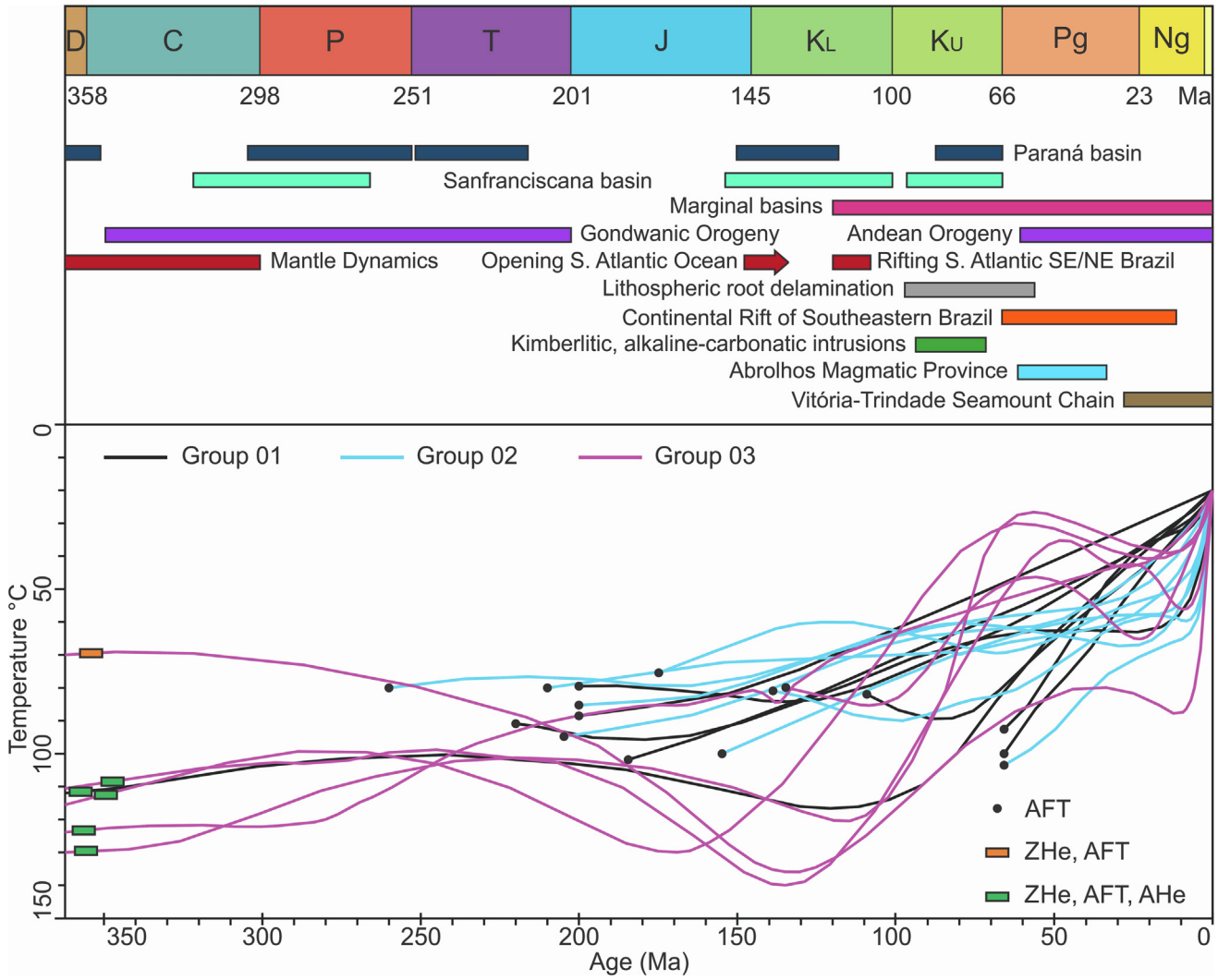

Fig. 3. Chronological chart evidencing the expected model weighted mean trajectories of the new thermal histories provided in this study, along with the leading local and regional events (sedimentary deposition, tectonism, mantle dynamics, and magmatism).

Portions of the Araçuaí Orogen that are far from the coast display Lower to Upper Cretaceous ages. The samples closer to the margin exhibit Upper Cretaceous to Paleogene ages, and some samples located to the northwest of latitude 20° S and longitude 40° W record ages varying from the Lower to Upper Cretaceous.

Furthermore, the AROS demonstrate a noticeable trend of decreasing AFT ages towards the coast, in some areas presenting Neogene ages close to the ocean. Contrasting to the overall ages of the Araçuaí Orogen, the Ribeira Orogen mainly displays Upper Cretaceous to Paleogene ages, with some Neogene ages in its southern portion. Some localized sites within the Ribeira Orogen display AFT ages from the Lower Cretaceous.

Finally, the intersection between the Ribeira and the southern Brasília orogens displays Jurassic to Lower Cretaceous ages, except its northerly region, which records Paleozoic and Triassic ages, and a site of Upper Cretaceous ages in the Brasília Orogen near an alkaline massif (Fig. 1).

The IDW maps (Figs. 5, 6, and 7), generated from the combined dataset, provide us with valuable insights into the temperature evolution within our study area. However, it is important to note that when it comes to temperature data predating the Mesozoic, we must acknowledge that some regions have limited available information, and the existing data may be relatively imprecise.

The SFC has consistently exhibited temperatures below 120 °C since the Paleozoic. Its southern segment has experienced temperatures lower than 80 °C since at least the Carboniferous, contrasting to the neighboring orogens. On the other hand, the northern SFC recorded temperatures ranging from 110 to 70 °C during the Paleozoic. During the Triassic to Jurassic, the temperature of the northern SFC was between 80 and 50 °C. At the same time, the transitional region of the craton with the northern Araçuaí Orogen near the margin remained at temperatures varying from 120 and 80 °C. From the Cretaceous (150 Ma map) onwards, the craton slowly cooled until the present-day surface conditions.

On the one hand, the portion of the Araçuaí Orogen near the present-day margin lacks thermal information before 180–150 Ma, resulted from temperatures higher than the range of the APAZ caused by continuous crustal erosion. On the other hand, the thermal history of the continent's interior derived from the AFT method dates further to the Carboniferous because of the relative thermal stability of the craton in the Mesozoic and the Cenozoic. Localized sites within the transitional region of the northern Araçuaí Orogen and SFC exhibit temperatures close to 110 °C from 210 to 150 Ma. During the Mesozoic to the Cenozoic, from 150 to 60 Ma, some sites were in higher temperatures, nearly 110 °C, while others cooled down to 50 °C. Finally, from 60 to 30 Ma, the

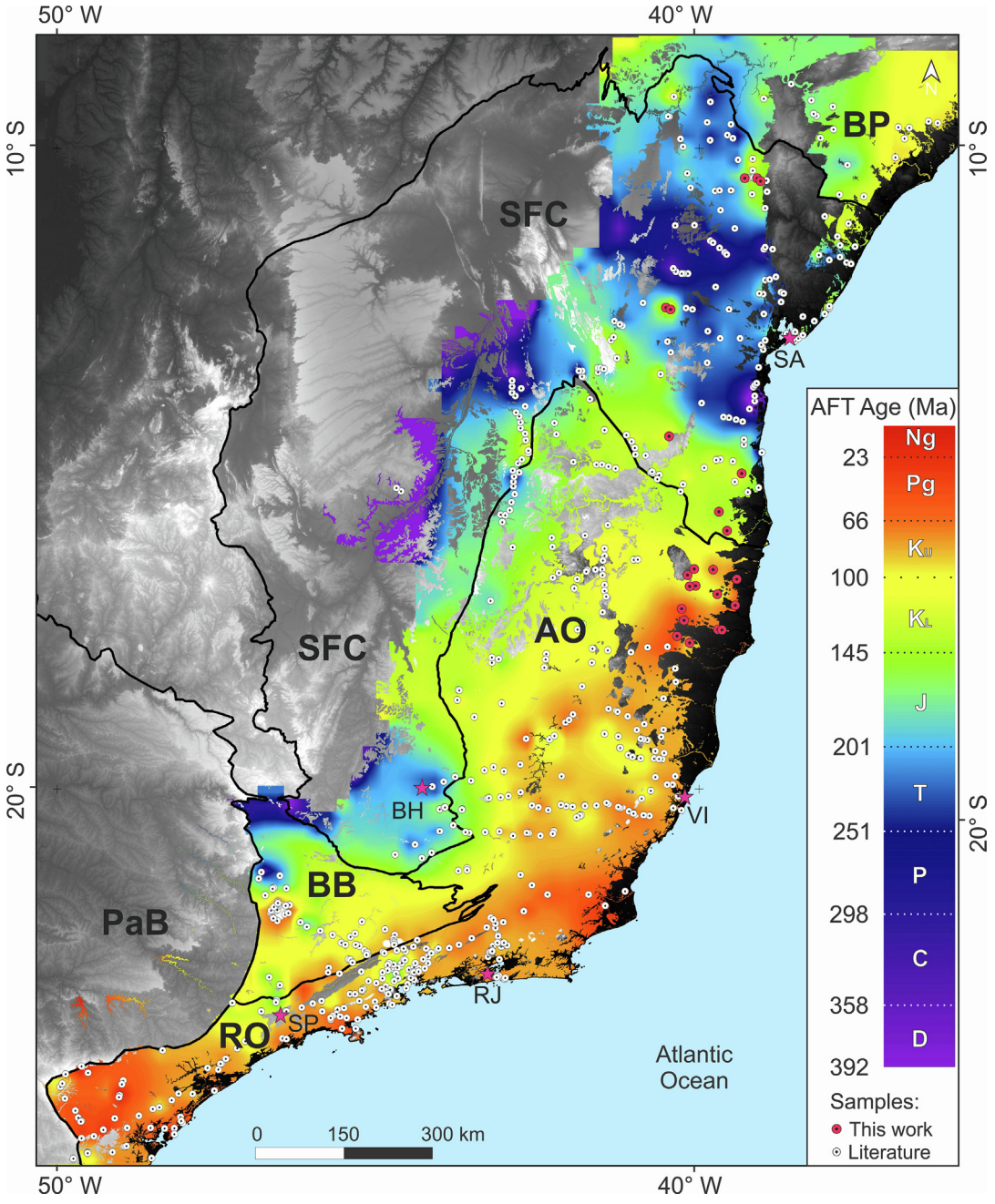

Fig. 4. Inverse distance weighted (IDW) map displaying the spatial distribution of Apatite Fission Track central ages in southeastern to northeastern Brazil. The interpolation process considered samples from Gallagher et al. (1994), Amaral et al. (1997), Harman et al. (1998), Cupertino (2000), Oliveira et al. (2000), Hadler et al. (2001), Tello Saenz et al. (2003), Carmo (2005), Franco et al. (2005), Ribeiro et al. (2005, 2011), Silva (2006), Hackspacher et al. (2007), Genaro (2008), Turner et al. (2008), Franco-Magalhaes et al. (2010, 2014), Hiruma et al. (2010), Gomes (2011), Cogné et al. (2012), Japsen et al. (2012), Doranti-Tiritan (2013), Karl et al. (2013), Jelinek et al. (2014, 2020), Souza et al. (2014), Engelmann de Oliveira et al. (2016), Soares et al. (2016), Amaral-Santos et al. (2019), Krob et al. (2019), Van Ranst et al. (2020), Fonseca et al. (2020, 2021, 2022, 2023), Gezatt et al. (2021), and Costa (2022). Samples from the Phanerozoic cover were not considered for interpolation. Abbreviations are: SFC: São Francisco Craton; AO: Araçuaí Orogen; RO: Ribeira Orogen; BB: Brasília Orogen; BP: Borborema Province; PaB: Paraná Basin; RJ: Rio de Janeiro City; SA: Salvador City; BH: Belo Horizonte City; After Engelmann de Oliveira and Jelinek (2017), Hueck et al. (2019), and Novo et al. (2021).

northern Araçuaí Orogen and the Ribeira Orogen display localized sites recording high temperatures of approximately 90 °C while the remaining portions of these orogens and the SFC display temperatures of approximately 50 °C or lower.

The temperature records in the Ribeira Orogen varied from 20 °C to over 180 °C during the Carboniferous to Triassic periods. The southern region had near surface temperatures at that time, while the northern region had higher temperatures of around 120 °C. During the Mesozoic, the contrasting temperatures between the northern and southern portions of the orogen remained. From 150 Ma onwards until present, some portions of this orogen display a temperature increment towards the Paraná Basin and then cooling to surface conditions, while some segments kept the temperatures nearly 90 °C until 90 to 60 Ma, followed by cooling.

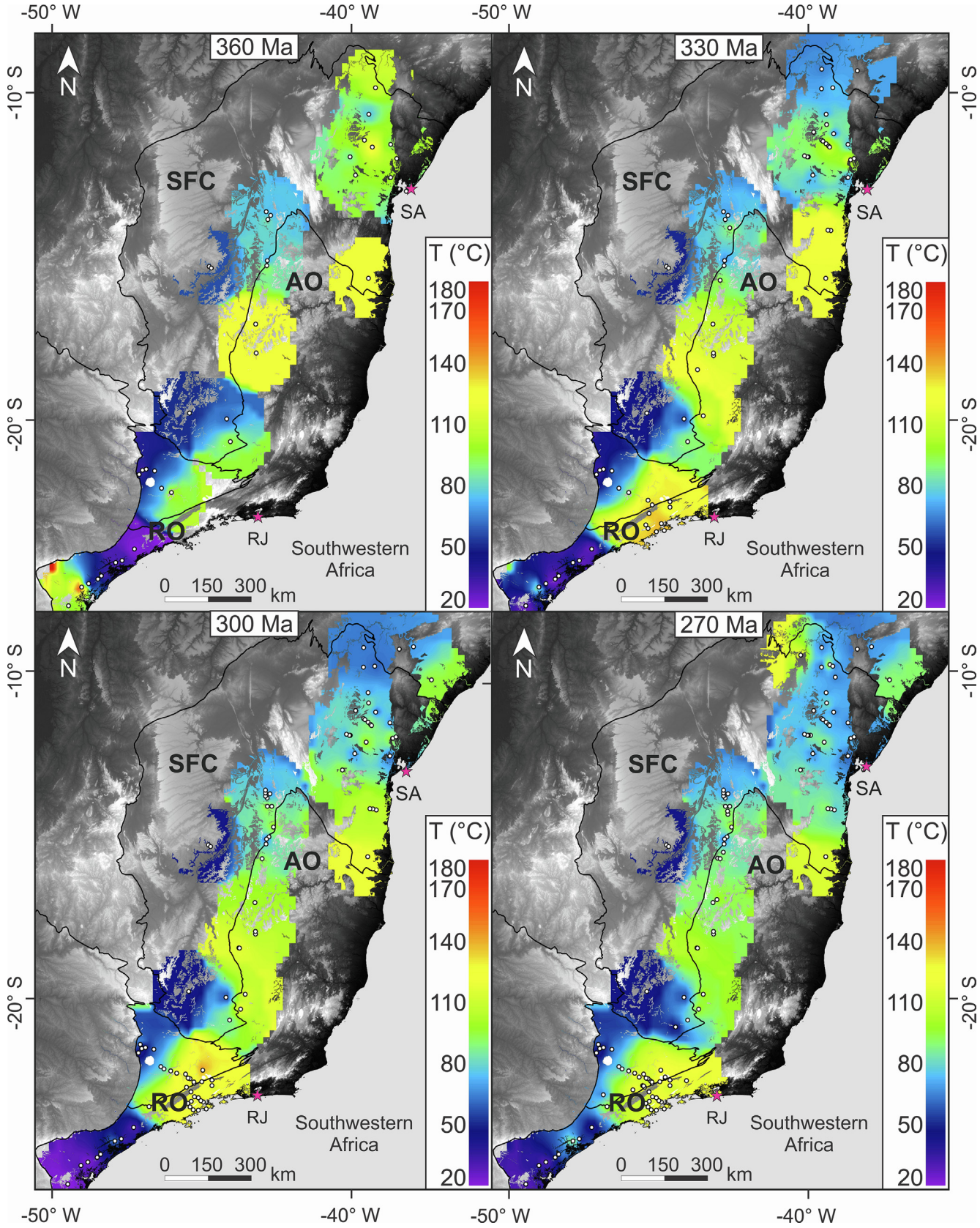

Fig. 5. Inverse distance weighted maps created through the interpolation of data collected from thermal models of basement samples across the São Francisco Craton (SFC), Araçuaí Orogen (AO), and Ribeira Orogen (RO) from 360 to 270 Ma. The time–temperature points collected from this work and samples available in the literature are displayed in Supplementary Data, Table S4. Pink stars refer to the state capital city. Abbreviations are: RJ: Rio de Janeiro City; SA: Salvador City; BH: Belo Horizonte City. (For interpretation of the references to colour in this figure legend, the reader is referred to the web version of this article.)

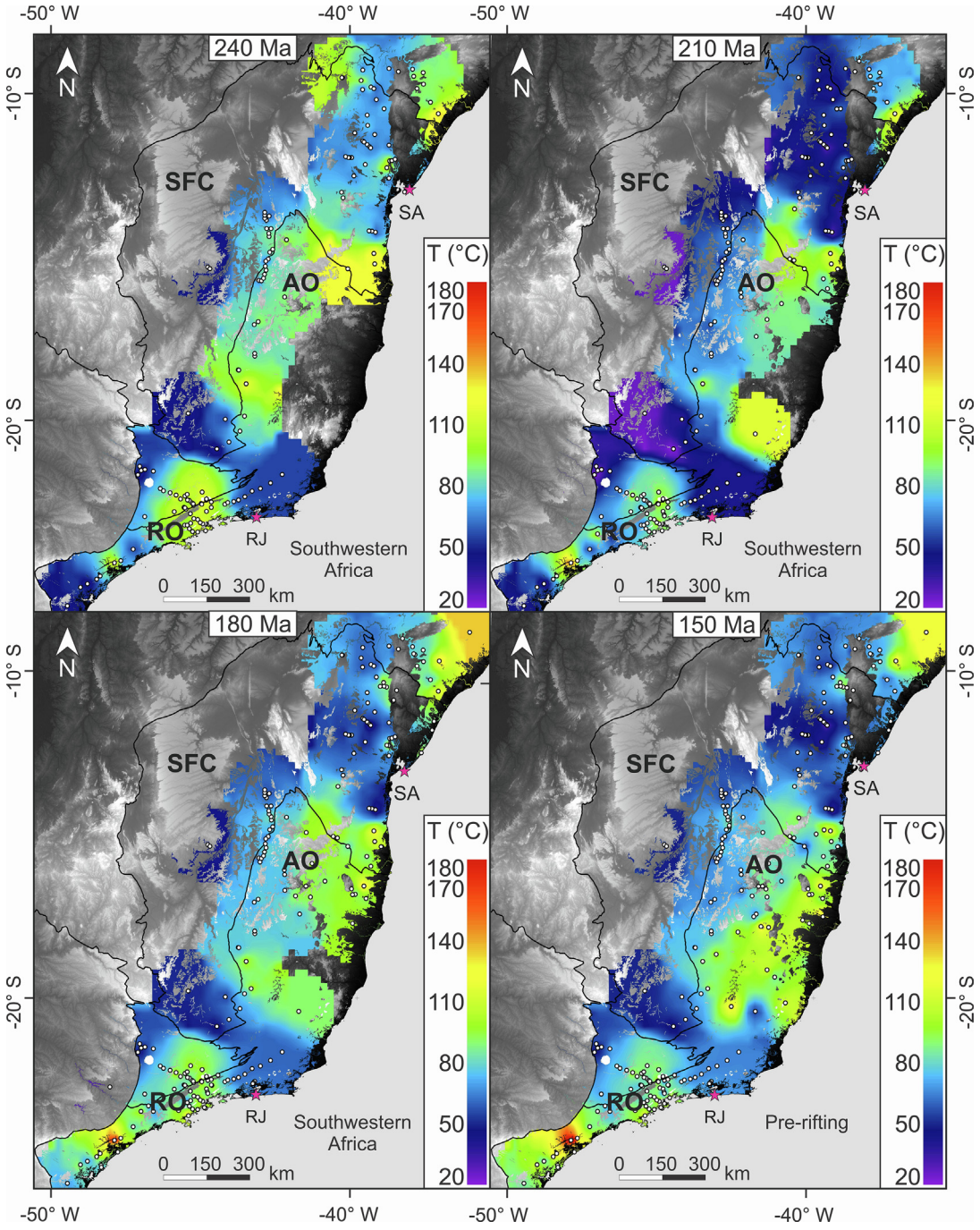

Fig. 6. Inverse distance weighted maps created through the interpolation of data collected from thermal models of basement samples across the São Francisco Craton (SFC), Araçuaí Orogen (AO), and Ribeira Orogen (RO) from 240 to 150 Ma. The time–temperature points collected from this work and samples available in the literature are displayed in Supplementary Data, Table S4. Pink stars refer to the state capital city. Abbreviations are: RJ: Rio de Janeiro City; SA: Salvador City; BH: Belo Horizonte City. (For interpretation of the references to colour in this figure legend, the reader is referred to the web version of this article.)

5. Thermotectonic assessment of the São Francisco Craton and surrounding orogens

5.1. The northern Araçuaí Orogen and São Francisco Craton: The new AFT data set

This study presents 23 new AFT central ages distributed across the northern AROS and the SFC (Tab. 2 and Fig. 2). We also provide 22 inverse thermal models (Fig. 3 and Supplementary Data, Fig. S5).

The new samples yield AFT ages from the Mesozoic to the Cenozoic, of which the AROS samples record younger AFT ages, and the SFC samples yield older AFT ages. This AFT data set negatively correlates to MTL and may represent the left portion of a boomerang plot (Green, 1986), indicating reset ages. The samples having MTL larger than 12 μm, i.e., intermediate to long track lengths, have noticeably young ages, characterizing the samples that were reset. We attribute the volcanism of the Abrolhos Magmatic Province during the Paleocene to the Eocene as the cause of the reset, evi-

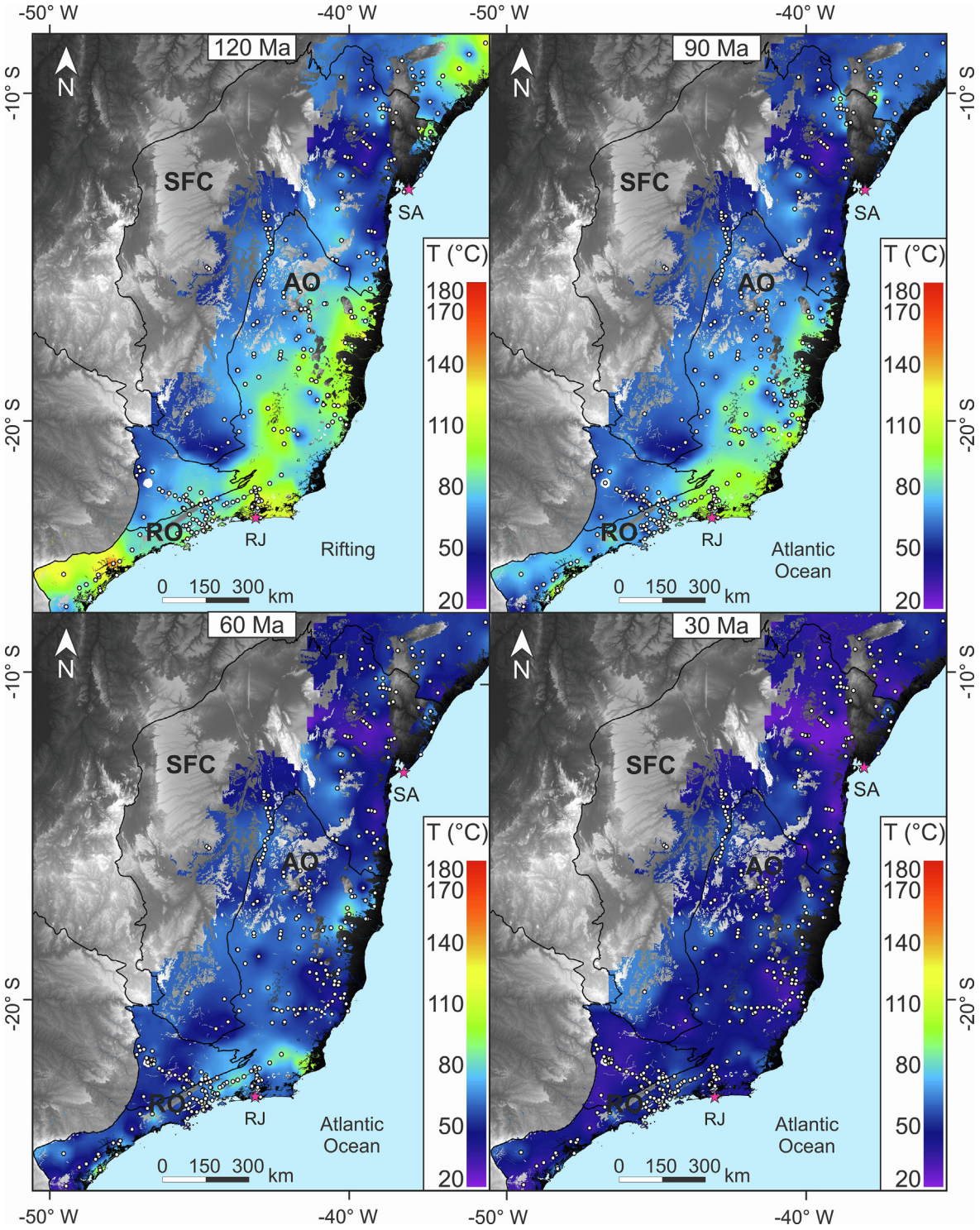

Fig. 7. Inverse distance weighted maps created through the interpolation of data collected from thermal models of basement samples across the São Francisco Craton (SFC), Araçuaí Orogen (AO), and Ribeira Orogen (RO) from 120 to 30 Ma. The time–temperature points collected from this work and samples available in the literature are displayed in Supplementary Data, Table S4. Pink stars refer to the state capital city. Abbreviations are: RJ: Rio de Janeiro City; SA: Salvador City; BH: Belo Horizonte City. (For interpretation of the references to colour in this figure legend, the reader is referred to the web version of this article.)

denced by the young AFT data presented here and the AHe ages obtained by do Amaral Santos et al. (2022).

Additionally, the negative skewing of most samples can correlate to a brief reheating event or extended residence within the APAZ. Considering this information, if reheating occurs, the extended residence in the APAZ, and within the range of the AHe thermochronometer (ca. 70 to 40 °C), leads apatites to be more retentive for α particles, causing their retention zone to undergo a temperature increment (Flowers et al., 2009), driving the AHe thermochronometer to hold slightly similar temperature bound-

aries with the AFT method. Therefore, this causes apatites to record similar ages in both methods and even to invert AHe and AFT ages (Flowers and Kelley, 2011), which is the case of a few samples in this study (BHS-02 and BHS-13) and some samples of Van Ranst et al. (2020) collected in the Araçuaí Orogen.

The intermediate to long MTL (12.5 to 13.2 μm) of samples of this study and their narrow standard deviation are indicative of fast cooling, which the thermal histories of samples BHS-02, 03, 04, 06, 08, 10, 13, and 15 show during the Cenozoic. Some of these samples, such as BHS-02, 06, 10, and 15, along with BHS-09 and 18, display accelerated cooling that is compatible with the time of rifting at 120 Ma, causing exhumation and sediment deposition in the new basins formed (Fig. 4).

Samples BHS-04, 08, 11, and 16 to 23 (Fig. 4), mainly located within the São Francisco Craton or close to its borders, exhibit a Paleogene-Neogene cooling event, which finds support in increased sedimentary thickness in the marginal basins (e.g. Jelinek et al., 2014).

5.2. The São Francisco Craton and Araçuaí-Ribeira orogenic system: Regional assessment

In this study, we compiled AFT data from 728 sites to create a IDW map illustrating the distribution of AFT ages (Fig. 4) in southeastern Brazil. Furthermore, for 357 samples, the thermal history (Fig. 3) allowed the compilation of thermal information to construct 12 IDW maps covering the time range from 360 to 30 Ma (Figs. 5, 6, and 7). The novel compilation highlighted in this research facilitates identifying and analyzing regional cooling patterns within the studied area.

5.2.1. Carboniferous to Triassic

During the Carboniferous to the Triassic, the SFC and AROS (e.g. Jelinek et al., 2014; Amaral-Santos et al., 2019; Fonseca et al., 2021; do Amaral Santos et al., 2022), along with other segments of West Gondwana (e.g., Kasanzu et al., 2016; Machado et al., 2019; Martins-Ferreira et al., 2020; do Amaral Santos et al., 2023), underwent cooling and erosion due to (1) intraplate stresses of the Gondwanic Orogenic Cycle (Fig. 3; Milani and Ramos, 1998) and (2) uplift caused by mantle dynamics (Dávila et al., 2023). During this time, the Santa Fé Group, the initial unit of the intracontinental Sanfranciscana Basin (Figs. 1 and 3), was deposited (Campos and Dardenne, 1997). This unit, dating back to the Carboniferous-Permian, consists of formations associated with periglacial environments (Sgarbi and de Sgarbi, 2001; Zalán and Silva, 2007), and its sediments were transported from the adjacent Brasiliano orogens (Linol et al., 2015). The IDW map recording the Paleozoic thermal signals (Fig. 5) provides supporting evidence that the majority of the SFC had already reached temperatures below 100 °C, with specific nuclei registering temperatures of 50 °C or below, indicating shallow portions of the crust or even surface exposure in the region where these samples were collected. The AFT ages spatial distribution (Fig. 4) within the SFC also sheds light on the cooling, as these ages represent the oldest data in the analyzed data set, reinforcing that the SFC remained relatively unaffected by rapid exhumation since at least the Carboniferous. Furthermore, the new MTL data of this study depict short to intermediate fission tracks for most of the SFC, suggesting long residence within the thermal range of the AFT method, thus implying slow cooling (samples BHS-11 and 16 to 23).

The lithosphere of the Araçuaí Orogen bordering the SFC exhibits intermediate AFT ages (Jurassic to Lower Cretaceous) compared to the coastal region, which shows younger Upper Cretaceous to Cenozoic AFT ages (Figs. 2 and 4). This disparity can be attributed to the gradual and slow continuous cooling observed in the inland portion of the Araçuaí Orogen towards the SFC, as evidenced by the temperature variations from the Carboniferous to the Permian (Fig. 5). In contrast, the eastern segment of the orogen, including the northern Ribeira Orogen, displays significantly younger AFT ages and lacks the thermal signal from the AFT method. This behavior is attributed to the likelihood that temperatures during that period likely exceeded 120 °C in the Araçuaí Orogen rocks. In such cases, thermochronometers with higher closure temperatures, such as zircon fission track (ZFT), should be utilized to access Paleozoic temperature information. Notably, the contrasting AFT ages between the SFC and the adjacent orogens depict a cooling control based on rheology, where the robust cratonic lithosphere tends to erode slowly. In contrast, the warmer and weaker orogenic lithosphere is rapidly removed (Fonseca et al., 2021).

The IDW maps (Fig. 5) also reveal a Paleozoic cooling in the basement of the Ribeira Orogen during the Carboniferous to the end of the Permian in a region adjacent to the Paraná Basin (Fig. 3). This basin served as an intracontinental depocenter in the West Gondwana continent during the Paleozoic to Upper Cretaceous (Milani et al., 2007a). The western portion of the Ribeira Orogen and the central Brasilia Orogen experienced temperatures comparable to the present-day surface conditions and then underwent erosion. The sediments from these regions contributed to the formation of the lower supersequences within the Paraná Basin (Milani et al., 2007a). In contrast, the eastern portion of the Ribeira Orogen and the southern tip of the Brasília Orogen were exposed to higher temperatures, delineating a boundary between the Santos Block to the north and the Peruíbe Block to the south due to the segmentation of these blocks by transfer zones (Fig. 1; Krob et al., 2019; Meisling et al., 2001). The basement near-surface exposure of the southern/central Ribeira Orogen can also be attributed to time–temperature constraints imposed during the inversion process, which compel the models to operate in low temperatures (Krob et al., 2019), which, in this case, we disregard, considering the geologic data record mentioned above.

5.2.2. Triassic to Jurassic

During the Triassic to Jurassic (240–180 Ma maps, Fig. 6), certain sections of the Araçuaí Orogen still experienced temperatures higher than the detectable range of the AFT thermochronometer (Fig. 6). The absence of thermal signals from both the AFT and AHe methods indicates posterior significant crustal erosion, where the shallow portion of the crust was continually eroded, along with the accompanying thermal records it once held. This hypothesis of deeply eroded lithosphere finds support in the exposure of high-grade metamorphic rocks, such as amphibolites to granulites, which form the crystalline core of the Araçuaí Orogen (Uhlein et al., 1998).

The thermal records pointed out by do Amaral Santos et al. (2022) and Hiruma et al. (2010) suggest that the end of the Gondwanic cycle may lead to exhumation and cooling in some portions of the AROS, bringing samples to shallow portions of the crust. After entering the APAZ, these samples started recording the AFT method, observed in the 150 Ma-map (Figs. 4 and 6).

Since 240 Ma, an estimated exhumation of 3,000–4,000 m can be inferred in the transition area of the northern Araçuaí Orogen and the SFC considering the temperatures observed in the compiled data (Fig. 6), and the geothermal gradient of 25 °C.km^{-1}. The sediments resulting from this exhumation were deposited in nearby basin depocenters, including the Sanfranciscana, Parnaíba, Recôncavo-Tucano-Jatobá basins (Milani et al., 2007b). These estimates align with those provided by Harman et al. (1998), Jelinek et al. (2014), and do Amaral Santos et al. (2022).

5.2.3. Late Jurassic-Early Cretaceous and Cenozoic

Starting from 150 Ma onwards, most of the samples examined in this study detected the thermal signal of the AFT. Samples BHS-14 and BHS-16 recorded AFT central ages dating from the Upper Jurassic to Lower Cretaceous (Fig. 2 and Supplementary Data, Fig. S5), suggesting that some samples were already within the APAZ. The interpolated maps (Figs. 4, 6, and 7) illustrate a distinct temperature and AFT age spatial distribution pattern attributed to the rheological difference between cratonic and non-cratonic lithosphere, as previously proposed by Fonseca et al. (2021, 2022) and supported in this study, which evidence differential cooling and exhumation. This pattern is evident in the contrasting temperatures of the Araçuaí Orogen and the craton: the northeastern AROS and transitional SFC display higher temperatures (110–80 °C), with localized sites exceeding this temperature range. In contrast, the inland Araçuaí Orogen and most of the SFC experienced lower temperatures (80–50 °C) (Fig. 3). The Borborema Province and the southern/central Ribeira Orogen exhibited higher temperatures than the SFC, supporting the assumption of differential exhumation based on rheology, since they are also composed of orogenic lithosphere. As stated in section 4.2, the AFT central age spatial distribution is another source of validation for the hypothesis of contrasting rheology leading to differential lithospheric exhumation.

The IDW maps (Figs. 6 and 7) also indicate a temperature increment from 150 to 120 Ma in the transitional region of the AROS. This artifact can be attributed to the interpolation process, which considered only a few samples displaying lower temperatures at 150 Ma for interpolation. However, at 120 Ma, several samples in the vicinity of this region entered the APAZ recording high temperatures (100–110 °C), which induced the interpolation process to display high temperatures, overwriting the low-temperature record of a few samples, and exhibiting a generalized reheating phase in this region, which we disregard and attribute to a software artifact.

From 120 to 90 Ma (Fig. 7), the region extending from Rio de Janeiro city to the north, up to the border with the SFC, underwent rapid cooling from 120 °C to nearly 70 °C. The new data set displays AFT ages that correlate to this event, which is the case of samples BH-01, BHS-08, BHS-09, and BHS-14. This accelerated cooling event is primarily attributed to the erosion of the rift shoulders formed in the Araçuaí Orogen (Jelinek et al., 2014; do Amaral Santos et al., 2022). The uplifted crystalline rocks, which comprise the shoulders, contributed sediments that were subsequently deposited in the adjacent basins – Campos, Espírito Santo, and Mucuri basins – within the newly opened Atlantic Ocean (Fig. 4). These sediments formed a sedimentary pile that reached a thickness of up 4,400 m (França et al., 2007a, 2007b; Winter et al., 2007). It is essential to notice that some samples of the cratonic domain also display AFT ages that can correlate to the Lower Cretaceous cooling event (samples BHS-11 and BHS-21), pointing to local cooling and erosion of the cratonic lithosphere to a lesser extent than observed for the orogenic lithosphere.

During the Upper Cretaceous onward, the South American plate was under a state of compression: at the Pacific margin, the plate changed its state from extension to compression, inducing shortening and exhumation in the Andes (Ramos, 2010); at the South Atlantic spreading center, the half-spreading rate increased, resulting in accentuated ridge-push (Torsvik et al., 2009). Coeval to this far-field stresses, in southeastern Brazil, numerous high-temperature intrusions, alkaline bodies, and kimberlites emplaced and erupted surrounding the São Francisco Craton (Ferreira et al., 2022; Gernon et al., 2023; Takenaka et al., 2023). Additionally, by the end of the Paleogene to Neogene, the Vitória-Trindade Seamount Chain located offshore in the Atlantic Ocean started erupting. These magmatic records suggest an increased heat flow in the area, making the crust thermally weak (Cogné et al., 2012; Japsen et al., 2012) and promoting surface uplift, which is also attributed to delamination of deep lithospheric roots (Hu et al., 2018). These heat sources, along with the combined far-field effects of plate borders and intraplate tectonism/epeirogeny, lead to deformation across the continent, driving exhumation, cooling, and sedimentary deposition in the marginal basins (Cogné et al., 2012).

At 60 Ma, the IDW map presented in this study (Fig. 7) shows temperatures of 70 °C, indicating that mostly the entire study area was at shallow crust portions. However, certain regions still exhibited higher temperatures, reaching nearly 100 °C (Fig. 7). This is observed in the Continental Rift of Southeastern Brazil (Riccomini et al., 2004) and the onshore region near the Abrolhos Magmatic Province (Stanton et al., 2021) (Figs. 1 and 3).

In the Ribeira Orogen, the CRSB installation zone experienced tectonic stress, potentially resulting in higher temperatures than its surroundings. Near the coast, temperatures of 90–100 °C are indicative of the Paleogene tectonism of the Guaraqueçaba, Cananéia, and Sete Barras grabens (Figs. 1 and 7; de Souza et al., 1996; Riccomini et al., 2004; Nascimento, 2013). Moreover, although the CRSB is primarily controlled by NE-SW shear zones (Giro et al., 2021), the Guaraqueçaba region exhibits multiple NW-SE lineaments associated with the Ponta Grossa Arch (dos Santos et al., 2023) in the southern Ribeira Orogen, which influence the drainage pattern and exhibit incised river channels (Nascimento, 2013; Salamuni et al., 2004). Furthermore, Hiruma et al. (2010) also argue that tectonism and fault reactivation caused changes in the drainage network and river capture during the Neogene, resulting in progressive denudation in the central Ribeira Orogen (Riccomini and Grohmann, 2010). In the northern Ribeira Orogen near the CRSB, reactivation of the shear zones caused the high-temperature regime observed in the IDW map at 60 Ma (Fig. 7), which also could be caused by sedimentation of the Cenozoic basins, as argued by Krob et al. (2019) and Salamuni et al. (2004), and the presence of alkaline intrusions (Fig. 1) heating its vicinity. Therefore, we propose that both the southern and northern Ribeira Orogen experienced higher temperatures, as indicated by noticeably young AFT ages (Fig. 3), due to post-rift reactivation of these lineaments and shear zones during CRSB development and locally increased temperatures due to the eruption of kimberlitic and alkaline-carbonatitic rocks nearby.

The onshore region of the northern Araçuaí Orogen, adjacent to the Abrolhos Magmatic Province (Fig. 1), depicts higher temperatures at 60 Ma (Fig. 7), evidencing cooling since then, and it contains some of the younger AFT samples of the Araçuaí Orogen (Table 2; samples BHS-02 to BHS-05, BHS-07, and BHS-15 in this study), ranging from 65 to 37 Ma. These young ages and high temperatures can be attributed to offshore volcanism in the Abrolhos Magmatic Province, primarily occurring between 56 and 37 Ma (Stanton et al., 2021) along with the presence of NW-SE lineaments that may have been reactivated and acted as conduits for heat transport, keeping the low-temperature thermochronometers opened, as previously advocated by do Amaral Santos et al. (2022) and supported by our findings.

At 30 Ma, the continental margin, mainly the interior of the SFC, and the inland section of the adjacent orogens were exposed at shallow to near-surface levels (Fig. 7). Using the methods employed in this study and those documented in the literature, an estimated exhumation of approximately 1,000 m has occurred from 30 Ma to the present. However, based on stratigraphic data, this thickness can vary from 500 m to more than 2,000 m, with the most significant sedimentary accumulation in the Espírito Santo Basin (França et al., 2007b), located to the east of the Araçuaí Orogen, and more minor accumulations the Camamu and Almada basins close to Salvador city and to the east of the SFC (Caixeta et al., 2007; Gontijo et al., 2007). To constrain the basement cooling

during the last 30 Ma, thus at shallow depths and cool temperatures, a lower-temperature thermochronometer would be required, such as Monazite Fission Track dating (Jones et al., 2021), which can lead to potential future studies in the area to constrain the time of rapid and slow cooling in the continent.

The results presented in this work, both new and compiled data, reinforce the importance of studying the transitional region of the SFC and AROS, considering the effects of differing rheology on the spatial distribution of AFT ages and exhumation. Specifically, the SFC's strong and cold cratonic lithosphere contrasts with the weak and warm orogenic lithosphere of the orogenic system. It is essential to highlight that certain regions, such as the southern Ribeira Orogen and the continental margin of the Araçuaí Orogen near the Abrolhos Magmatic Province, may exhibit local rapid exhumation and reheating episodes (Fig. 7). These phenomena can be attributed to post-rift tectonism through fault reactivation and the effects of volcanism and heating transport along faults that were coevally acting upon the lithosphere.

6. Conclusion

In conclusion, our research has shed light on several critical aspects of the thermochronological evolution and exhumation history of the São Francisco Craton (SFC) and the adjacent Araçuaí-Ribeira orogenic system (AROS). Through the analysis of apatite fission track ages (AFT), ranging from 154.4 ± 20.1 to 37.1 ± 3.0 Ma, and temperature data, we have identified significant variations in the thermal history of these regions, which have been instrumental in understanding the tectonic processes and geological evolution that have shaped them.

One key finding is the contrasting behavior between the cratonic lithosphere of the São Francisco Craton and the orogenic lithosphere of the AROS. The strong and cold cratonic lithosphere erodes slowly, while the weak and warm orogenic lithosphere is continuously removed. This stark contrast is reflected in the AFT ages and thermal records, providing valuable insights into the dynamics of lithospheric processes.

Additionally, volcanic activity and fault reactivation have played crucial roles in the thermal evolution of specific areas. Firstly, during the rift phase of the South Atlantic Ocean opening, the exhumation of elevated rift shoulders caused cooling in the AROS. Offshore volcanism in the Abrolhos Magmatic Province, located to the west of the Araçuaí Orogen and SFC, between 56 and 37 Ma, has contributed to elevated temperatures in the onshore region of the northern Araçuaí Orogen. Additionally, post-rift tectonic processes, including fault reactivation and volcanism near the Continental Rift of Southeastern Brazil, as well as eruption of kimberlitic, alkaline-carbonatitic rocks and the Vitória-Trindade Seamount Chain have led to local rapid exhumation and reheating episodes both in the Ribeira Orogen and the continental margin near the Abrolhos Magmatic Province.

These findings contribute to a better understanding of the geodynamic evolution of the São Francisco Craton and AROS and have implications for regional tectonic models and the exploration of natural resources in these areas. The observed variations in thermal history provide valuable insights into the dynamics of lithospheric processes, highlighting the need for comprehensive studies that integrate thermochronological data with other geological and geophysical observations.

CRediT authorship contribution statement

Edgar do Amaral Santos: Conceptualization, Methodology, Validation, Formal analysis, Investigation, Writing – original draft, Visualization. **Andréa Ritter Jelinek:** Conceptualization, Methodology, Formal analysis, Writing – review & editing, Supervision, Project administration, Funding acquisition. **Frederico Antônio Genezine:** Formal analysis, Resources. **Daniel Stockli:** Formal analysis, Resources.

Declaration of Competing Interest

The authors declare that they have no known competing financial interests or personal relationships that could have appeared to influence the work reported in this paper.

Acknowledgments

E. Amaral Santos thanks the Ph.D. scholarship provided by the Conselho Nacional de Desenvolvimento Científico e Tecnológico – CNPq (140775/2019-6). A.R. Jelinek thanks to the Conselho Nacional de Desenvolvimento Científico e Tecnológico - CNPq (Project 309329/2020-5). The authors thank the Associate Editor of Gondwana Research, Dr. Andrea Festa, and two anonymous reviewers who contributed enormously to improving this work's early version.

While preparing this work, the authors used ChatGPT to review the English grammar and word spelling. After using this service, the authors reviewed and edited the content as needed and took full responsibility for the publication's content.

Appendix A. Supplementary material

Supplementary data to this article can be found online at https://doi.org/10.1016/j.gr.2023.12.003.

References

Alkmim, F.F., Kuchenbecker, M., Reis, H.L.S., 2017. The Araçuaí Belt. In: Heilbron, M., Cordani, U.G., Alkmim, F.F. (Eds.), São Francisco Craton, Eastern Brazil. Springer, Cham, pp. 255–276. https://doi.org/10.1007/978-3-319-01715-0.

Alkmim, F.F., Marshak, S., 1998. Transamazonian Orogeny in the Southern São Francisco Craton Region, Minas Gerais, Brazil: Evidence for Paleoproterozoic collision and collapse in the Quadrilátero Ferrífero. Precambrian Res. 90, 29–58. https://doi.org/10.1016/s0301-9268(98)00032-1.

Alkmim, F.F., Marshak, S., Pedrosa-Soares, A.C., Peres, G.G., Cruz, S.C.P., Whittington, A., 2006. Kinematic evolution of the Araçuaí-West Congo orogen in Brazil and Africa: Nutcracker tectonics during the Neoproterozoic assembly of Gondwana. Precambrian Res. 149, 43–64. https://doi.org/10.1016/j.precamres.2006.06.007.

Alkmim, F.F., Martins-Neto, M.A., 2012. Proterozoic first-order sedimentary sequences of the São Francisco craton, eastern Brazil. Mar. Pet. Geol. 33, 127–139. https://doi.org/10.1016/j.marpetgeo.2011.08.011.

Amaral, G., Born, H., Hadler, J.C.N., Iunes, P.J., Kawashita, K., Machado, D.L., Oliveira, E.P., Paulo, S.R., Tello, C.A.S., 1997. Fission track analysis of apatites from São Francisco craton and Mesozoic alcaline-carbonatite complexes from central and southeastern Brazil. J. South Am. Earth Sci. 10, 285–294. https://doi.org/10.1016/s0895-9811(97)00020-5.

Amaral-Santos, E., Jelinek, A.R., Almeida-Abreu, P.A., Genezine, F.A., 2019. Phanerozoic cooling history of Archean/Paleoproterozoic basement in the southern Espinhaço Range, southeastern Brazil, through apatite fission-track analysis. J. South Am. Earth Sci. 96,. https://doi.org/10.1016/j.jsames.2019.102352 102352.

Caixeta, J.M., Da Silva Milhomem, P., Witzke, R.E., Siqueira Dupuy, I.S., Gontijo, G.A., 2007. Bacia de Camamu. Bol. Geociencias da Petrobras 15, 455–461.

Campos, J.E.G., Dardenne, M.A., 1997. Estratigrafia E Sedimentação Da Bacia Sanfranciscana: Uma Revisão. Rev. Bras. Geociências 27, 269–282. https://doi.org/10.25249/0375-7536.1997269282.

Carlson, W.D., Donelick, R.A., Ketcham, R.A., 1999. Variability of apatite fission-track annealing kinetics: I. Experimental results. Am. Mineral. 84, 1213–1223. https://doi.org/10.2138/am-1999-0901.

Carmo, I.D., 2005. Geocronologia do intemperismo Cenozoico no Sudoeste do Brasil. Dep. Geol. Universidade Federal do Rio de Janeiro.

Chang, H.K., Kowsmann, R.O., Figueiredo, A.M.F., Bender, A.A., 1992. Tectonics and stratigraphy of the East Brazil Rift system: an overview. Tectonophysics 213, 97–138. https://doi.org/10.1016/0040-1951(92)90253-3.

Cogné, N., Gallagher, K., Cobbold, P.R., 2011. Post-rift reactivation of the onshore margin of southeast Brazil: Evidence from apatite (U–Th)/He and fission-track data. Earth Planet. Sci. Lett. 309, 118–130. https://doi.org/10.1016/j.epsl.2011.06.025.

Cogné, N., Gallagher, K., Cobbold, P.R., Riccomini, C., Gautheron, C., 2012. Post-breakup tectonics in southeast Brazil from thermochronological data and

combined inverse-forward thermal history modeling. J. Geophys. Res. B Solid Earth 117, 1–16. https://doi.org/10.1029/2012JB009340.
Costa, D., 2022. Late Cretaceous exhumation of the Doce River valley and the Colatina Fracture Zone, Southeastern Brazil: implications from apatite fission-track data. Universidade Federal de Minas Gerais.
Cupertino, J.A., 2000. Evolução tectono-climática na fase Rifte das bacias de Camamu, parte norte, e sul do Recôncavo, com ênfase na utilização de isótopos estáveis e traços de fissão. Universidade Federal do Rio Grande do Sul.
Dalton de Souza, J., Kosin, M., Melo, R.C., Santos, R.A., Teixeira, L.R., Sampaio, A.R., Guimarães, J.T., Vieira Bento, R., Borges, V.P., Martins, A.A.M., Arcanjo, J.B., Loureiro, H.S.C., Angelim, L.A.A., 2003. Mapa Geológico do Estado da Bahia - Escala 1:1.000.000.
Dávila, F.M., Martina, F., Ávila, P., Ezpeleta, M., 2023. Mantle contribution to Late Paleozoic glaciations of SW Gondwana. Glob. Planet. Change 220,. https://doi.org/10.1016/j.gloplacha.2022.104018 104018.
de Almeida, F.F.M., 1977. O Cráton do São Francisco. Rev. Bras. Geociências 7, 349–364.
de Oliveira, S.G., Hackspacher, P.C., Hadler Neto, J.C., Iunes, P.J., de Paulo, S.R., Ribeiro, L.F.B., Tello Saenz, C.A., 2000. Constraints on the Evolution and Thermal History of the Continental Platform of Southeast Brazil, São Paulo State, Using Apatite Fission Track Analysis (Afta). Rev. Bras. Geociências 30, 107–109. https://doi.org/10.25249/0375-7536.2000301107109.
de Souza, D.H., Hackspacher, P.C., Doranti-Tiritan, C., De Godoy, D.F., 2014. Comparação Da Dinâmica Evolutiva, a Longo E Curto Prazo, Entre O Planalto De Poços De Caldas E O Planalto De São Pedro De Caldas. Rev. Bras. Geomorfol. 15, 251–272. https://doi.org/10.20502/rbg.v15i2.481.
de Souza, L.A.P., Tessler, M.G., Galli, V.L., 1996. O Gráben De Cananéia. Rev. Bras. Geociências 26, 139–150. https://doi.org/10.25249/0375-7536.1996139150.
Degler, R., Pedrosa-Soares, A., Dussin, I., Queiroga, G., Schulz, B., 2017. Contrasting provenance and timing of metamorphism from paragneisses of the Araçuaí-Ribeira orogenic system, Brazil: Hints for Western Gondwana assembly. Gondwana Res. 51, 30–50. https://doi.org/10.1016/j.gr.2017.07.004.
do Amaral Santos, E., Jelinek, A.R., Machado, J.P., Stockli, D., 2022. Thermal history along the Araçuaí Orogen and São Francisco Craton border, eastern Brazilian continental margin, based on low-temperature thermochronologic data. Tectonophysics 825, 229232. https://doi.org/10.1016/j.tecto.2022.229232.
do Amaral Santos, E., Jelinek, A.R., Stockli, D., Genezine, F.A., 2023. Contrasting thermal histories in the Dom Feliciano Belt triggered by magmatism related to the Paraná-Etendeka LIP and fracture zone proximity. Tectonophysics 857, 229841. https://doi.org/10.1016/j.tecto.2023.229841.
Donelick, R.A., O'Sullivan, P.B., Ketcham, R.A., 2005. Apatite fission-track analysis, in: Reiners, P.W., Ehlers, T.A. (Eds.), Reviews in Mineralogy and Geochemistry. pp. 49–94. https://doi.org/10.2138/rmg.2005.58.3.
Doranti-Tiritan, C., 2013. Evolução geomórfica e modelagem termocinemática 3D da região do planalto de Poços de Caldas (SP/MG). Universidade Estadual Paulista.
dos Santos, J.M., Salamuni, E., Morales, N., de Castro, L.G., Lima da Silva, C., de Souza, I.A., Gimenez, V.B., Oliveira, S.P., 2023. Aeromagnetic and structural characterization of dyke swarms in southeast Brazil: Evidence for Cenozoic reactivation of the Guapiara lineament, Ponta Grossa Arch. J. South Am. Earth Sci. 129,. https://doi.org/10.1016/j.jsames.2023.104523 104523.
Engelmann de Oliveira, C.H., Jelinek, A.R., 2017. História termotectônica da margem continental Brasileira a partir de dados de traços de fissão em apatita. Pesqui. em Geociencias 44, 387–400. https://doi.org/10.22456/1807-9806.83263.
Engelmann de Oliveira, C.H., Jelinek, A.R., Chemale, F., Cupertino, J.A., 2016. Thermotectonic history of the southeastern Brazilian margin: Evidence from apatite fission track data of the offshore Santos Basin and continental basement. Tectonophysics 685, 21–34. https://doi.org/10.1016/j.tecto.2016.07.012.
Ferreira, A.C.D., Conceição, R.V., Mizusaki, A.M.P., 2022. Mesozoic to Cenozoic alkaline and tholeiitic magmatism related to West Gondwana break-up and dispersal. Gondwana Res. 106, 15–33. https://doi.org/10.1016/j.gr.2022.01.005.
Fleischer, R.L., Price, P.B., 1964. Techniques for geological dating of minerals by chemical etching of fission fragment tracks. Geochim. Cosmochim. Acta 28, 1705–1714. https://doi.org/10.1016/0016-7037(64)90017-1.
Flowers, R.M., Kelley, S.A., 2011. Interpreting data dispersion and "inverted" dates in apatite (U-Th)/He and fission-track data sets. Geochim. Cosmochim. Acta 75, 5169–5186. https://doi.org/10.1016/j.gca.2011.06.016.
Flowers, R.M., Ketcham, R.A., Shuster, D.L., Farley, K.A., 2009. Apatite (U-Th)/He thermochronometry using a radiation damage accumulation and annealing model. Geochim. Cosmochim. Acta 73, 2347–2365. https://doi.org/10.1016/j.gca.2009.01.015.
Fonseca, A., Cruz, S., Novo, T., He, Z., De Grave, J., 2022. Differential exhumation of cratonic and non-cratonic lithosphere revealed by apatite fission-track thermochronology along the edge of the São Francisco craton, eastern Brazil. Sci. Rep. 12, 2728. https://doi.org/10.1038/s41598-022-06419-w.
Fonseca, A.C.L., Novo, T.A., Nachtergaele, S., Fonte-Boa, T.M.R., Van Ranst, G., De Grave, J., 2021. Differential Phanerozoic evolution of cratonic and non-cratonic lithosphere from a thermochronological perspective: São Francisco Craton and marginal orogens (Brazil). Gondwana Res. 93, 106–126. https://doi.org/10.1016/j.gr.2021.01.006.
Fonseca, A., Novo, T., Fonte-Boa, T., Kuchenbecker, M., Fragoso, D.G.C., Peifer, D., Pedrosa-Soares, A.C., De Grave, J., 2023. Control of inherited structural fabric on the development and exhumation of passive margins – Insights from the Araçuaí Orogen (Brazil). Geosci. Front. 14,. https://doi.org/10.1016/j.gsf.2023.101628 101628.
Fonseca, A.C., Piffer, G.V., Nachtergaele, S., Van Ranst, G., De Grave, J., Novo, T.A., 2020. Devonian to Permian post-orogenic denudation of the Brasília Belt of West Gondwana: insights from apatite fission track thermochronology. J. Geodyn. 137,. https://doi.org/10.1016/j.jog.2020.101733 101733.
França, R.L., Del Rey, A.C., Tagliari, C.V., Brandão, J.R., De Rossi Fontanelli, P., 2007a. Bacia de Mucuri. Bol. Geociencias da Petrobras 15, 493–499.
França, R.L., Del Rey, A.C., Tagliari, C.V., Brandão, J.R., De Rossi Fontanelli, P., 2007b. Bacia do Espírito Santo. Bol. Geociencias da Petrobras 15, 501–509.
Franco, A.O.B., Hackspacher, P.C., Godoy, D.F., Ribeiro, L.F.B., Guedes, S., 2005. História Térmica do Maciço Alcalino de Poços de Caldas (SP/MG) e adjacências através da análise de datação por traços de fissão em apatitas. Rev. Bras. Geociências 35, 351–358.
Franco-Magalhaes, A.O.B., Hackspacher, P.C., Glasmacher, U.A., Saad, A.R., 2010. Rift to post-rift evolution of a "passive" continental margin: The Ponta Grossa Arch, SE Brazil. Int. J. Earth Sci. 99, 1599–1613. https://doi.org/10.1007/s00531-010-0556-8.
Franco-Magalhaes, A.O.B., Cuglieri, M.A.A., Hackspacher, P.C., Saad, A.R., 2014. Long-term landscape evolution and post-rift reactivation in the southeastern Brazilian passive continental margin: Taubaté basin. Int. J. Earth Sci. 103, 441–453. https://doi.org/10.1007/s00531-013-0967-4.
Galbraith, R.F., 1981. On statistical models for fission track counts. J. Int. Assoc. Math. Geol. 13, 471–478. https://doi.org/10.1007/BF01034498.
Gallagher, K., 2012. Transdimensional inverse thermal history modeling for quantitative thermochronology. J. Geophys. Res. Solid Earth 117, B02408. https://doi.org/10.1029/2011JB008825.
Gallagher, K., Hawkesworth, C.J., Mantovani, M.S.M., 1994. The denudation history of the onshore continental margin of SE Brazil inferred from apatite fission track data. J. Geophys. Res. 99, 117–145. https://doi.org/10.1029/94jb00661.
Genaro, D.T., 2008. Contrubuição ao Conhecimento de Processos Atuantes no Rifteamento Continental, por Traços de Fissão em Zircões e Apatitas, Aplicados no Rift Continental do Sudeste do Brasil, Bacias de Taubaté, Resende, Volta Redonda e Circunvizinhanças. Universidade Estadual Paulista.
Gernon, T.M., Jones, S.M., Brune, S., Hincks, T.K., Palmer, M.R., Schumacher, J.C., Primiceri, R.M., Field, M., Griffin, W.L., O'Reilly, S.Y., Keir, D., Spencer, C.J., Merdith, A.S., Glerum, A., 2023. Rift-induced disruption of cratonic keels drives kimberlite volcanism. Nature 620. https://doi.org/10.1038/s41586-023-06193-3.
Gezatt, J.N., Macdonald, D.I.M., Stephenson, R., Jelinek, A.R., Carter, A., 2021. South Atlantic passive margin evolution: A thermochronology case study from the Rio de Janeiro-Três Rios section, SE Brazil. J. South Am. Earth Sci. 106,. https://doi.org/10.1016/j.jsames.2020.103051 103051.
Giro, J.P., Almeida, J., Guedes, E., Bruno, H., 2021. Tectonic inheritances in rifts: The meaning of NNE lineaments in the continental rift of SE-Brazil. J. South Am. Earth Sci. 108,. https://doi.org/10.1016/j.jsames.2021.103225 103225.
Gleadow, A.J.W., Duddy, I.R., 1981. A natural long-term track annealing experiment for apatite. Nucl. Tracks 5, 169–174. https://doi.org/10.1016/0191-278X(81)90039-1.
Gleadow, A.J.W., Duddy, I.R., Green, P.F., Hegarty, K.A., 1986. Fission track lengths in the apatite annealing zone and the interpretation of mixed ages. Earth Planet. Sci. Lett. 78, 245–254. https://doi.org/10.1016/0012-821X(86)90065-8.
Gomes, C.H., 2011. História Térmica Das Regiões Sul E Sudeste Da América Do Sul: Implicações Na Compartimentação Geotectônica Do Gondwana. Cristiane Heredia Gomes. Universidade Federal do Rio Grande do Sul.
Gontijo, G.A., Da Silva Milhomem, P., Caixeta, J.M., Siqueira Dupuy, I.S., De Lemos Menezes, P.E., 2007. Bacia de Almada. Bol. Geociencias da Petrobras 15, 463–473.
Green, P.F., 1986. On the thermo-tectonic evolution of Northern England: Evidence from fission track analysis. Geol. Mag. 123, 493–506. https://doi.org/10.1017/S0016756800035081.
Green, P.F., Duddy, I.R., Gleadow, A.J.W., Tingate, P.R., Laslett, G.M., 1986. Thermal Annealing of Fission Tracks in Apatite: 1. A Qualitative Description. Chem. Geol. Isot. Geosci. Sect. 59, 237–253. https://doi.org/10.1016/0168-9622(86)90074-6.
Green, P.F., Duddy, I.R., Laslett, G.M., Hegarty, K.A., Gleadow, A.J.W., Lovering, J.F., 1989. Thermal annealing of fission tracks in apatite 4. Quantitative modelling techniques and extension to geological timescales. Chem. Geol. Isot. Geosci. Sect. 79, 155–182. https://doi.org/10.1016/0168-9622(89)90018-3.
Guenthner, W.R., Reiners, P.W., Ketcham, R.A., Nasdala, L., Giester, G., 2013. Helium diffusion in natural zircon: radiation damage, anisotropy, and the interpretation of zircon (U-TH)/He thermochronology. Am. J. Sci. 313, 145–198. https://doi.org/10.2475/03.2013.01.
Hackspacher, P.C., de Godoy, D.F., Ribeiro, L.F.B., Hadler Neto, J.C., Franco, A.O.B., 2007. Modelagem térmica e geomorfologia da borda sul do Cráton do São Francisco: termocronologia por traços de fissão em apatita. Rev. Bras. Geociências 37, 76–86. https://doi.org/10.25249/0375-7536.200737s47686.
Hadler, J.C., Paulo, S.R., Iunes, P.J., Tello, S.C.A., Balestrieri, M.L., Bigazzi, G., Curvo, E.A.C., Hackspacher, P., 2001. A PC compatible Brazilian software for obtaining thermal histories using apatite fission track analysis. Radiat. Meas. 34, 149–154. https://doi.org/10.1016/S1350-4487(01)00141-X.
Harman, R., Gallagher, K., Brown, R., Raza, A., Bizzi, L., 1998. Accelerated denudation and tectonic/geomorphic reactivation of the craton of northeastern Brazil during the Late Cretaceous. J. Geophys. Res. 103, 27091–27105.
Heilbron, M., Eirado, L.G., Almeida, J., 2016. Mapa geológico e de recursos minerais do estado do Rio de Janeiro. Escala 1:400.000. Programa Geol. do Bras. CPRM.
Heilbron, M., Cordani, U.G., Alkmim, F.F., 2017a. The São Francisco Craton and Its Margins, in: Heilbron, M., Cordani, U.G., Alkmim, F.F. (Eds.), São Francisco Craton, Eastern Brazil. Springer, Cham, pp. 3–13. https://doi.org/10.1007/978-3-319-01715-0_1.

Heilbron, M., Ribeiro, A., Valeriano, C.M., Paciullo, F. V, Almeida, J.C.H., Trouw, R.J.A., Tupinambá, M., Silva, L.G.E., 2017b. The Ribeira Belt, in: Heilbron, M., Cordani, U.G., Alkmim, F.F. (Eds.), São Francisco Craton, Eastern Brazil. Springer, Cham, pp. 277–302. https://doi.org/10.1007/978-3-319-01715-0.

Heilbron, M., de Morisson Valeriano, C., Peixoto, C., Tupinambá, M., Neubauer, F., Dussin, I., Corrales, F., Bruno, H., Lobato, M., Horta de Almeida, J.C., Guilherme do Eirado Silva, L., 2020. Neoproterozoic magmatic arc systems of the central Ribeira belt, SE-Brazil, in the context of the West-Gondwana pre-collisional history: A review. J. South Am. Earth Sci. 103, 102710. https://doi.org/10.1016/j.jsames.2020.102710.

Heilbron, M., Machado, N., 2003. Timing of terrane accretion in the Neoproterozoic-Eopaleozoic Ribeira Orogen (SE Brazil). Precambrian Res. 125, 87–112. https://doi.org/10.1016/S0301-9268(03)00082-2.

Hiruma, S.T., Riccomini, C., Modenesi-Gauttieri, M.C., Hackspacher, P.C., Neto, J.C.H., Franco-Magalhães, A.O.B., 2010. Denudation history of the Bocaina Plateau, Serra do Mar, southeastern Brazil: Relationships to Gondwana breakup and passive margin development. Gondwana Res. 18, 674–687. https://doi.org/10.1016/j.gr.2010.03.001.

Hu, J., Liu, L., Faccenda, M., Zhou, Q., Fischer, K.M., Marshak, S., Lundstrom, C., 2018. Modification of the Western Gondwana craton by plume-lithosphere interaction. Nat. Geosci. 11, 203–210. https://doi.org/10.1038/s41561-018-0064-1.

Hueck, M., Dunkl, I., Heller, B., Stipp Basei, M.A., Siegesmund, S., 2018. (U-Th)/He Thermochronology and Zircon Radiation Damage in the South American Passive Margin: Thermal Overprint of the Paraná LIP? Tectonics 37, 4068–4085. https://doi.org/10.1029/2018TC005041.

Hueck, M., Dunkl, I., Oriolo, S., Wemmer, K., Basei, M.A.S., Siegesmund, S., 2019. Comparing contiguous high- and low-elevation continental margins: New (U-Th)/He constraints from South Brazil and an integration of the thermochronological record of the southeastern passive margin of South America. Tectonophysics 770,. https://doi.org/10.1016/j.tecto.2019.228222 228222.

Hurford, A.J., 1990. International Union of Geological Sciences: Subcommission on Geochronology recommendation for the standardization of fission track dating calibration and data reporting. Int. J. Radiat. Appl. Instrumentation. Part 17, 233–236. https://doi.org/10.1016/1359-0189(86)90061-0.

Hurford, A.J., Green, P.F., 1983. The zeta age calibration of fission-track dating. Chem. Geol. 41, 285–317. https://doi.org/10.1016/S0009-2541(83)80026-6.

Japsen, P., Bonow, J.M., Green, P.F., Cobbold, P.R., Chiossi, D., Lilletveit, R., Magnavita, L.P., Pedreira, A., 2012. Episodic burial and exhumation in NE Brazil after opening of the South Atlantic. Bull. Geol. Soc. Am. 124, 800–816. https://doi.org/10.1130/B30515.1.

Jelinek, A.R., Chemale, F., van der Beek, P.A., Guadagnin, F., Cupertino, J.A., Viana, A., 2014. Denudation history and landscape evolution of the northern East-Brazilian continental margin from apatite fission-track thermochronology. J. South Am. Earth Sci. 54, 158–181. https://doi.org/10.1016/j.jsames.2014.06.001.

Jelinek, A.R., Corrêa-Gomes, L.C., Bicca, M.M., 2020. Evolução termotectônica fanerozoica da margem continental na área do Rifte Recôncavo-Tucano-Jatobá. Pesqui. em Geociências 47, e0823.

Jepson, G., Carrapa, B., Gillespie, J., Feng, R., DeCelles, P.G., Kapp, P., Tabor, C.R., Zhu, J., 2021. Climate as the Great Equalizer of Continental-Scale Erosion. Geophys. Res. Lett. 48, e2021GL095008. https://doi.org/10.1029/2021GL095008.

Jones, S., Gleadow, A., Kohn, B., 2021. Thermal annealing of implanted 252Cf fission tracks in monazite. Geochronology 3, 89–102. https://doi.org/10.5194/gchron-3-89-2021.

Karl, M., Glasmacher, U.A., Kollenz, S., Franco-Magalhaes, A.O.B., Stockli, D.F., Hackspacher, P.C., 2013. Evolution of the South Atlantic passive continental margin in southern Brazil derived from zircon and apatite (U-Th-Sm)/He and fission-track data. Tectonophysics 604, 224–244. https://doi.org/10.1016/j.tecto.2013.06.017.

Kasanzu, C.H., Linol, B., de Wit, M.J., Brown, R., Persano, C., Stuart, F.M., 2016. From source to sink in central Gondwana: Exhumation of the Precambrian basement rocks of Tanzania and sediment accumulation in the adjacent Congo basin. Tectonics 35, 2034–2051. https://doi.org/10.1002/2016TC004147.

Ketcham, R.A., Carter, A., Donelick, R.A., Barbarand, J., Hurford, A.J., 2007. Improved modeling of fission-track annealing in apatite. Am. Mineral. 92, 799–810. https://doi.org/10.2138/am.2007.2281.

Kohn, B., Chung, L., Gleadow, A., 2019. Fission-Track Analysis: Field Collection, Sample Preparation and Data Acquisition. Springer International Publishing. https://doi.org/10.1007/978-3-319-89421-8_2.

Krob, F.C., Glasmacher, U.A., Karl, M., Perner, M., Hackspacher, P.C., Stockli, D.F., 2019. Multi-chronometer thermochronological modelling of the Late Neoproterozoic to recent t-T-evolution of the SE coastal region of Brazil. J. South Am. Earth Sci. 92, 77–94. https://doi.org/10.1016/j.jsames.2019.02.012.

Linol, B., de Wit, M.J., Milani, E.J., Guillocheau, F., Scherer, C., 2015. New Regional Correlation Between the Congo, Paraná and Cape-Karoo Basins of Southwest Gondwana. In: Wit, D.e., Maarten, J., Guillocheau, F., De Wit, M.C.J. (Eds.), Geology and Resource Potential of the Congo Basin. Springer, Berlin, Heidelberg, pp. 245–268. https://doi.org/10.1007/978-3-642-29482-2.

Machado, J.P.S.L., Jelinek, A.R., Bicca, M.M., Stephenson, R., Genezini, F.A., 2019. West Gondwana orogenies and Pangaea break-up: Thermotectonic effects on the southernmost Mantiqueira Province, Brazil. J. Geol. Soc. London. 176, 1056–1075. https://doi.org/10.1144/jgs2019-018.

Martins-Ferreira, M.A.C., Dias, A.N.C., Chemale, F., Campos, J.E.G., 2020. Intracontinental uplift of the Brazilian Central Plateau linked to continental breakup, orogenies, and basin filling, supported by apatite and zircon fission-track data. Arab. J. Geosci. 13, 891. https://doi.org/10.1007/s12517-020-05885-8.

Meisling, K.E., Cobbold, P.R., Mount, V.S., 2001. Reactivation of an obliquely rifted margin, Campos and Santos basins, southeastern Brazil. Am. Assoc. Pet. Geol. Bull. 85, 1903–1924. https://doi.org/10.1306/8626d0b3-173b-11d7-8645000102c1865d.

Milani, E.J., Faccini, U.F., Scherer, C.M., Araújo, L.M., Cupertino, J.A., 1998. Sequences and stratigraphic hierarchy of the Paraná Basin (Ordovician to Cretaceous), southern Brazil. Bol. IG-USP. Série Científica 29, 125–173. https://doi.org/10.11606/issn.2316-8986.v29i0p125-173.

Milani, E.J., Gonçalves De Melo, J.H., De Souza, P.A., Fernandes, L.A., França, A.B., 2007a. Bacia do Paraná. Bol. Geociencias da Petrobras 15, 265–287.

Milani, E.J., Ramos, V.A., 1998. Paleozoic orogenies in southwestern Gondwana and the subsidence cycles of the Parana Basin. Rev. Bras. Geociências 28, 473–484.

Milani, E.J., Rangel, H.D., Bueno, G.V., Stica, J.M., Winter, W.R., Caixeta, J.M., Da Cruz Pessoa Neto, O., 2007b. Bacias sedimentares brasileiras - Cartas estratigráficas. Bol. Geociencias da Petrobras 15, 183–205.

Mohriak, W.U., Fainstein, R., 2012. Phanerozoic regional geology of the eastern Brazilian margin. In: Roberts, D.G., Bally, A.W. (Eds.), Regional Geology and Tectonics: Phanerozoic Passive Margins, Cratonic Basins and Global Tectonic Maps. Elsevier, Boston, pp. 222–282. https://doi.org/10.1016/B978-0-444-56357-6.00006-8.

Mohriak, W., Nemčok, M., Enciso, G., 2008. South Atlantic divergent margin evolution: Rift-border uplift and salt tectonics in the basins of SE Brazil. Geol. Soc. Spec. Publ. 294, 365–398. https://doi.org/10.1144/SP294.19.

Nascimento, E.R. do, 2013. Morfotectônica E Origem Das Morfoestruturas Da Serra Do Mar Paranaense. Universidade Federal do Paraná.

Novo, T.A., Fonte-boa, T.M.R., Rolim, J.M., Fonseca, A.C., 2021. The state of the art of low-temperature thermochronometry in Brazil. J. Geol. Surv. Brazil 4, 239–256. https://doi.org/10.29396/jgsb.2021.v4.n3.4.

Nürnberg, D., Müller, R.D., 1991. The tectonic evolution of the South Atlantic from Late Jurassic to present. Tectonophysics 191, 27–53. https://doi.org/10.1016/0040-1951(91)90231-G.

Oriolo, S., Oyhantçabal, P., Wemmer, K., Siegesmund, S., 2017. Contemporaneous assembly of Western Gondwana and final Rodinia break-up: Implications for the supercontinent cycle. Geosci. Front. 8, 1431–1445. https://doi.org/10.1016/j.gsf.2017.01.009.

Pedrosa-Soares, A.C., Noce, C.M., Wiedemann, C.M., Pinto, C.P., 2001. The Araçuaí-West-Congo Orogen in Brazil: An overview of a confined orogen formed during Gondwanaland assembly. Precambr. Res. 110, 307–323. https://doi.org/10.1016/S0301-9268(01)00174-7.

Pedrosa-Soares, A.C., Alkmim, F.F., Tack, L., Noce, C.M., Babinski, M., Silva, L.C., Martins-Neto, M.A., 2008. Similarities and differences between the Brazilian and African counterparts of the Neoproterozoic Araçuaí-West Congo orogen. Geol. Soc. Spec. Publ. 294, 153–172. https://doi.org/10.1144/SP294.9.

Pedrosa-Soares, A.C., Wiedemann-Leonardos, C.M., 2000. Evolution of Araçuaí Belt and its connection to the Ribeira Belt, eastern Brazil, in: Cordani, U.G., Milani, E. J., Thomaz-Filho, A., Campos, D.A. (Eds.), Tectonic Evolution of South America. 31st International Geological Congress, Rio de Janeiro, pp. 265–285. https://doi.org/10.13140/2.1.3802.5928.

Pedrosa-Soares, A.C., DE Campos, C.P., Noce, C., Silva, L.C., Novo, T., Roncato, J., Medeiros, S., Castañeda, C., Queiroga, G., Dantas, E., Dussin, I., Alkmim, F., 2011. Late Neoproterozoic – Cambrian granitic magmatism in the Araçuaí orogen (Brazil), the Eastern Brazilian Pegmatite Province and related mineral resources. Geol. Soc. London Spec. Publ. 350, 25–51.

Perrota, M.M., Salvador, E.D., Lopes, R.C., D'Agostinho, L.Z., Peruffo, N., Gomes, S.D., Sachs, L.L.B., Meira, V.T., Garcia, M.G.M., Lacerda Filho, J. V., 2005. Mapa Geológico do Estado de São Paulo, escala 1:750.000.

Pinheiro, M.R., Cianfarra, P., 2021. Brittle deformation in the neoproterozoic basement of southeast brazil: Traces of intraplate cenozoic tectonics. Geosciences 11, 1–16. https://doi.org/10.3390/geosciences11070270.

Price, P.B., Walker, R.M., 1963. Fossil Tracks of Charged Particles in Mica and the Age of Minerals. J. Geophys. Res. 68, 4847–4862. https://doi.org/10.1029/JZ068i016p04847.

Ramos, V.A., 2010. The tectonic regime along the Andes: Present-day and Mesozoic regimes. Geol. J. 45, 2–25. https://doi.org/10.1002/gj.1193.

Reiners, P.W., Carlson, R.W., Renne, P.R., Cooper, K.M., Granger, D.E., McLean, N.M., Schoene, B., 2017. Diffusion and thermochronologic interpretations, in: Reiners, P.W., Carlson, R.W., Renne, P.R., Cooper, K.M., Granger, D.E., McLean, N.M., Schoene, B. (Eds.), Geochronology and Thermochronology. Wiley, pp. 83–126. https://doi.org/10.1002/9781118455876.ch5.

Ribeiro, L.F.B., Hackspacher, P.C., Ribeiro, M.C.S., Hadler Neto, J.C., Tello, S.C.A., Iunes, P.J., Franco, A.O.B., Godoy, D.F., 2005. Thermotectonic and fault dynamic analysis of Precambrian basement and tectonic constraints with the Parana basin. Radiat. Meas. 39, 669–673. https://doi.org/10.1016/j.radmeas.2004.09.007.

Ribeiro, M.C.S., Hackspacker, P.C., Ribeiro, L.F.B., Hadler Neto, J.C., 2011. Evolução Tectônica E Denudacional Da Serra Do Mar (Se/Brasil) No Limite Entre O Cretáceo Superior E Paleoceno, Utilizando Análises De Traços De Fissão E U-Th/He Em Apatitas. Rev. Bras. Geomorfol. 12, 3–14. https://doi.org/10.20502/rbg.v12i0.254.

Riccomini, C., 1990. O Rift continental do sudeste do Brasil. Universidade de São Paulo.

Riccomini, C., Grohmann, C.H., Sant'Anna, L.G., Hiruma, S.T., 2010. A captura das cabeceiras do Rio Tietê pelo Rio Paraíba do Sul, in: Modenesi-Gauttieri, M.C.,

Bartorelli, A., Carneiro, V.M.-N., Ré, C.D., Lisboa, M.B.D.A.L. (Eds.), A Obra de Aziz Nacib Ab'Sáber. Beca, São Paulo, pp. 157–169.
Riccomini, C., Gomes, L., Anna, S., 2004. Evolução geológica do rift continental do sudeste do Brasil, in: Mantesso-Neto, V., Bartorelli, A., Carneiro, C.D.R., Brito-Neves, B.B. de (Eds.), Geologia Do Continente Sul-Americano: Evolução Da Obra de Fernando Flávio de Almeida. Beca, pp. 383–405.
Riccomini, C., Velázquez, V.F., Gomes, C.B., 2005. Tectonic controls of the Mesozoic and Cenozoic alkaline magmatism in the central- southeastern Brazilian Platform. Mesozoic to Cenozoic Alkaline Magmat. Brazilian Platf. 31–57.
Salamuni, E., Ebert, H.D., Hasui, Y., 2004. Morfotectônica Da Bacia Sedimentar De Curitiba. Rev. Bras. Geociências 34, 469–478. https://doi.org/10.25249/0375-7536.2004344469478.
Sandwell, D.T., Müller, R.D., Smith, W.H.F., Garcia, E., Francis, R., 2014. New global marine gravity model from CryoSat-2 and Jason-1 reveals buried tectonic structure. Science (80-.) 346, 65–67. https://doi.org/10.1126/science.1258213.
Scherer, C.M.S., Reis, A.D., Horn, B.L.D., Bertolini, G., Lavina, E.L.C., Kifumbi, C., Goso Aguilar, C., 2023. The stratigraphic puzzle of the permo-mesozoic southwestern Gondwana: The Paraná Basin record in geotectonic and palaeoclimatic context. Earth-Science Rev. 240,. https://doi.org/10.1016/j.earscirev.2023.104397 104397.
Sgarbi, G.N.C., Sgarbi, P.B. de A., Campos, J.E.G., Dardenne, M.A., Penha, U.C., 2001. Bacia Sanfranciscana: o registro Fanerozóico da Bacia do São Francisco, in: Pinto, C.P., Martins-Neto, M.A. (Eds.), Bacia Do São Francisco: Geologia e Recursos Naturais. SBG/MG, pp. 93–138.
Silva, L.G.A.F., 2006. A interação entre os eventos tectônicos e a evolução geomorfológica da Serra da Bocaina. Universidade do Estado do Rio de Janeiro, Sudeste do Brasil.
Silva, M.A., Pinto, C.P., Pinheiro, M.A.P., Marinho, M.S., Lombello, J.C., Pinho, J.M.M.P., Goulart, L.E.A., Magalhães, J.R., 2020. Mapa Geológico do Estado de Minas Gerais, Escala 1:1.000.000.
Soares, C.J., Guedes, S., Jonckheere, R., Hadler, J.C., Passarella, S.M., Dias, A.N.C., 2016. Apatite fission-track of Cretaceous alkaline rocks of Ponta Grossa and Alto Paranaíba Arches, Brazil. Geol. J. 51, 805–810. https://doi.org/10.1002/gj.2694.
Souza, M.E., de Souza Martins, M., Queiroga, G.N., Leite, M., Oliveira, R.G., Dussin, I., Pedrosa-Soares, A.C., 2019. Paleoenvironment, sediment provenance and tectonic setting of Tonian basal deposits of the Macaúbas basin system, Araçuaí orogen, southeast Brazil. J. South Am. Earth Sci. 96,. https://doi.org/10.1016/j.jsames.2019.102393 102393.
Stanton, N., Gordon, A., Cardozo, C., Kusznir, N., 2021. Morphostructure, emplacement and duration of the Abrolhos Magmatic Province: A geophysical analysis of the largest post-breakup magmatism of the South-Eastern Brazilian margin. Mar. Pet. Geol. 133,. https://doi.org/10.1016/j.marpetgeo.2021.105230 105230.
Tagami, T., O'Sullivan, P.B., 2005. Fundamentals of fission-track thermochronology. Rev. Mineral. Geochemistry 58, 19–47. https://doi.org/10.2138/rmg.2005.58.2.
Takenaka, L.B., Förster, M.W., Alard, O., Griffin, W.L., Jacob, D.E., Basei, M.A.S., O'Reilly, S.Y., 2023. Multi-mineral geochronology of kimberlites, kamafugites and alkaline-carbonatite rocks, SW São Francisco Craton, Brazil: Appraisal of intrusion ages. Gondwana Res. 124, 246–272. https://doi.org/10.1016/j.gr.2023.05.012.
Tello Saenz, C.A., Hackspacher, P.C., Hadler Neto, J.C., Iunes, P.J., Guedes, S., Ribeiro, L.F.B., Paulo, S.R., 2003. Recognition of Cretaceous, Paleocene, and Neogene tectonic reactivation through apatite fission-track analysis in Precambrian areas of southeast Brazil: Association with the opening of the South Atlantic Ocean. J. South Am. Earth Sci. 15, 765–774. https://doi.org/10.1016/S0895-9811(02)00131-1.
Torsvik, T.H., Rousse, S., Labails, C., Smethurst, M.A., 2009. A new scheme for the opening of the South Atlantic Ocean and the dissection of an Aptian salt basin. Geophys. J. Int. 177, 1315–1333. https://doi.org/10.1111/j.1365-246X.2009.04137.x.
Turner, J.P., Green, P.F., Holford, S.P., Lawrence, S.R., 2008. Thermal history of the Rio Muni (West Africa)-NE Brazil margins during continental breakup. Earth Planet. Sci. Lett. 270, 354–367. https://doi.org/10.1016/j.epsl.2008.04.002.
Uhlein, A., Egydio-Silva, M., Bouchez, J.L., Vauchez, A., 1998. The Rubim pluton (Minas Gerais, Brazil): a petrostructural and magnetic fabric study. J. South Am. Earth Sci. 11, 179–189. https://doi.org/10.1016/S0895-9811(98)00009-1.
Val, P., Venerdini, A.L., Ouimet, W., Alvarado, P., Hoke, G.D., 2018. Tectonic control of erosion in the southern Central Andes. Earth Planet. Sci. Lett. 482, 160–170. https://doi.org/10.1016/j.epsl.2017.11.004.
Van Ranst, G., Pedrosa-Soares, A.C., Novo, T., Vermeesch, P., De Grave, J., 2020. New insights from low-temperature thermochronology into the tectonic and geomorphologic evolution of the south-eastern Brazilian highlands and passive margin. Geosci. Front. 11, 303–324. https://doi.org/10.1016/j.gsf.2019.05.011.
Vermeesch, P., 2009. RadialPlotter: A Java application for fission track, luminescence and other radial plots. Radiat. Meas. 44, 409–410. https://doi.org/10.1016/j.radmeas.2009.05.003.
Winter, W.R., Jahnert, R.J., França, A.B., 2007. Bacia de Campos. Bol. Geociencias da Petrobras 15, 511–529.
Zalán, P.V., De Oliveira, J.A.B., 2005. Origem e evolução estrutural do Sistema de Rittes Cenozóicos do Sudeste do Brasil (Origin and structural evolution of the Cenozoic Rift System of Southeastern Brasil). Bol. Geociencias da Petrobras 13, 269–300.
Zalán, P.V., Silva, P.C.R., 2007. Bacia do São Francisco. Bol. Geociencias da Petrobras 15, 561–571.